Properties and phenomena relevant to CH_4-CO_2 replacement in hydrate-bearing sediments

J. W. Jung,[1] D. Nicolas Espinoza,[1] and J. Carlos Santamarina[1]

Received 18 December 2009; revised 18 June 2010; accepted 29 June 2010; published 21 October 2010.

[1] The injection of carbon dioxide, CO_2, into methane hydrate-bearing sediments causes the release of methane, CH_4, and the formation of carbon dioxide hydrate, even if global pressure-temperature conditions remain within the CH_4 hydrate stability field. This phenomenon, known as CH_4-CO_2 exchange or CH_4-CO_2 replacement, creates a unique opportunity to recover an energy resource, methane, while entrapping a greenhouse gas, carbon dioxide. Multiple coexisting processes are involved during CH_4-CO_2 replacement, including heat liberation, mass transport, volume change, and gas production among others. Therefore, the comprehensive analysis of CH_4-CO_2 related phenomena involves physico-chemical parameters such as diffusivities, mutual solubilities, thermal properties, and pressure- and temperature-dependent phase conditions. We combine new experimental results with published studies to generate a data set we use to evaluate reaction rates, to analyze underlying phenomena, to explore the pressure-temperature region for optimal exchange, and to anticipate potential geomechanical implications for CH_4-CO_2 replacement in hydrate-bearing sediments.

Citation: Jung, J. W., D. N. Espinoza, and J. C. Santamarina (2010), Properties and phenomena relevant to CH_4-CO_2 replacement in hydrate-bearing sediments, *J. Geophys. Res.*, *115*, B10102, doi:10.1029/2009JB000812.

1. Introduction

[2] Global sustainability, in terms of energy needs and climate stress from greenhouse gases, requires new sources of energy and the management of CO_2 emissions. Methane hydrate is a potential energy source, with worldwide reserves on the order of 500–10,000 Gt of carbon [*Collett*, 2002; *Kvenvolden*, 1988; *Milkov*, 2004; *Ruppel and Pohlman*, 2008]. Methane can be recovered from hydrate-bearing sediments by depressurization, heating or chemical injection. In particular, the injection of carbon dioxide, CO_2, into hydrate-bearing sediments can liberate methane, CH_4, and sequester CO_2 in hydrate form [*McGrail et al.*, 2007; *Ota et al.*, 2005a; *Stevens et al.*, 2008; *Svandal et al.*, 2006; *Zhou et al.*, 2008a].

[3] The chemical potential difference between CH_4 and CO_2 hydrate indicates that CH_4-CO_2 gas replacement is thermodynamically favorable [*Seo and Lee*, 2001; *Svandal et al.*, 2006]. However, the extent of the reaction and its efficiency in real systems is determined by multiple factors and coexisting processes, such as (1) pressure and temperature-dependent solubilities and interfacial properties, (2) relative viscosity, permeability, and density between water and CO_2, (3) invasion patterns and specific surface of the hydrate phase, (4) fluid expansion after replacement, and (5) changes in effective stress. These phenomena couple to determine replacement efficiency and the geomechanical response of the sediment mass.

[4] In this study, we review previous CH_4-CO_2 replacement studies, identify and analyze underlying processes, present new experimental results, and anticipate potential implications.

2. Physical and Thermodynamic Properties

[5] The process of replacing CH_4 with CO_2 in hydrate must be understood at both the molecular scale and the macroscale to anticipate conditions for efficient CH_4-CO_2 replacement and its consequences on thermal, mechanical and electrical properties. In this section, we summarize physical parameters in tabular form and highlight the most relevant observations in the text.

2.1. Structure: Geometry and Length Scales

[6] Both CH_4 and CO_2 form structure I hydrate (Table 1a). This crystallographic structure is composed of 2 small cages for every 6 large cages, so the stoichiometric formula is $6X{\cdot}2Y{\cdot}46H_2O$, i.e., a maximum of 6 gas molecules X in large cages plus a maximum of 2 gas molecules Y in small cages, and 46 water molecules. The lattice repeats every ~12 Å [*Sloan and Koh*, 2008]. Thus, gas molecules make up a significant molar fraction ~15% of the hydrate structure (compare to the gas solubility in liquid water ~0.1% molar fraction, section 2.5).

[7] The stoichiometric ratio (number of water molecules per number of gas molecules) often deviates from the theoretical value $n = 46/8 = 5.75$ for structure I hydrate. In particular, the occupancy of CO_2 molecules in small cages

[1]School of Civil and Environmental Engineering, Georgia Institute of Technology, Atlanta, Georgia, USA.

0148-0227/10/2009JB000812

Table 1a. Physical Properties of CH_4 and CO_2 Hydrate, Pure CO_2 and Water Relevant to CH_4 Replacement by CO_2 in Hydrate-Bearing Sediments: Structure[a]

Property	CH_4 Hydrate (sI)	CO_2 Hydrate (sI)	CO_2 Liquid[b]	H_2O Liquid[b]
Stoichiometric ratio or hydration number, (number of H_2O molecules per number of gas molecules)	5.75 (100% cage occupancy)[c] (1); 5.81–6.10 [1.9–9.7 MPa, 263–285 K] (2)	5.75 (100% cage occupancy)[c] (1); 6.57 [1.5 MPa, 273 K] (3)		
Cage occupancy	~100% Large cage; ~70% Small cage; [10 MPa, 273 K] (3)	~100% Large cage; ~50% Small cage, [1.5 MPa, 273 K] (3)		
Cavity size (Å)	7.9, 8.66 (1)	7.9, 8.66 (1)		
Guest size (Å)	4.36 (1)	5.12 (1)		
Lattice constant *a* (Å)	11.95 [10 MPa, 271.15 K] (3)	12.07 [273.2 K] (4)		

[a]Numbers in parentheses indicate sources as follows: 1, *Sloan and Koh* [2008]; 2, *Circone et al.* [2005]; 3, *Klapproth et al.* [2003]; 4, *Uchida et al.* [1999].
[b]Refer to Figure 1.
[c]Computed value.

increases with pressure and the stoichiometric ratio decreases from ~6.6 at 1.3 MPa and 273.15 K, to a value closer to the theoretical limit 5.75 at 4.5 MPa and 283.15 K [*Anderson*, 2003; *Klapproth et al.*, 2003]. The CH_4 molecule is slightly smaller than CO_2 and fits more easily in small cages, so the stoichiometric ratio for CH_4 hydrate is typically n = 5.81–6.10 [*Circone et al.*, 2005]. As a result, the stoichiometric ratio of CH_4 hydrate is less sensitive to pressure than the stoichiometric ratio of CO_2 hydrate.

[8] Figure 1 shows hydrate-forming molecules and related molecular structures; they are drawn using the corresponding van der Waals radii and are shown at the same scale. The size of the opening between water molecules that form the face of big cages is smaller than the size of both CO_2 and CH_4 molecules. This simple observation leads us to conclude that the hydrate cage must separate to release the CH_4 molecule before it can trap CO_2. The molecule of nitrogen N_2 is smaller than CO_2 and fits more easily in the small cages of sI hydrate; this explains the enhanced CH_4 replacement efficiency obtained when a mixture of CO_2 and N_2 is used in a water-limited CH_4 hydrate system of structure I, or of structure II if combined with C_2H_6 [*Park et al.*, 2006].

2.2. Thermal Properties

[9] In agreement with Le Châtelier's principle, hydrate formation is an exothermic reaction (Table 1b). In particular, the heat liberated during the formation of a mol of CO_2 hydrate varies between $H^{f}_{CO2-hyd}$ = 57.7 and 63.6 kJ mol^{-1} (note that a mol of CO_2 hydrate is 44 g + n 18 g, where n = 5.75–6) [*Anderson*, 2003]. Conversely, hydrate dissociation is endothermic as heat is needed to disorganize the crystal structure. The heat adsorbed during the dissociation of a mol of CH_4 hydrate is H^{d}_{CH4hyd} = 52.7–55.4 kJ mol^{-1}, where a mol of CH_4 hydrate is 16 g + n 18 g and n~5.75 [*Anderson*, 2004]. Therefore, CH_4-CO_2 replacement is exothermic. The path assumed here involves complete CH_4 hydrate dissociation before CO_2 hydrate formation. Molecular dynamic simulations for CH_4-CO_2 replacement in the first monolayer (interface between CH_4 hydrate and liquid CO_2) show only partial dissociation of the hydrate cage and lower enthalpy change for the complete replacement reaction (B. Kvamme, personal communication, 2010). Experimental and numerical data are still needed to assess the evolution of the reaction when a large hydrate mass is involved, as in the pore space of sediments, where the characteristic length scale is much greater than the crystal nanometer scale.

[10] The thermal conductivity λ and diffusivity κ of liquid CO_2 are significantly lower than the corresponding values for either hydrates or water. In addition, water has the highest heat capacity c among all participating phases. This combination of thermal properties suggests reduced heat dissipation and increased local heating where liquid CO_2 displaces water and contacts CH_4 hydrate.

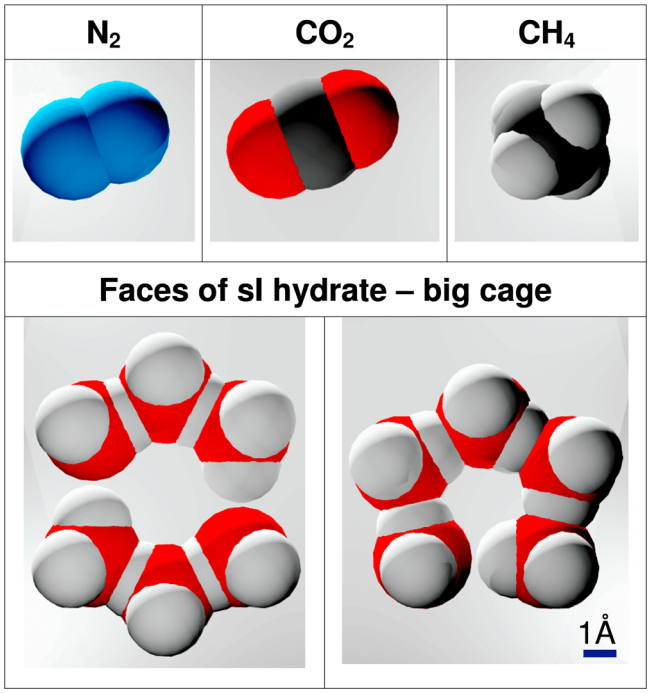

Figure 1. Hydrate-forming molecules (N_2, CO_2, and CH_4) and two faces of the big cage in sI hydrate. All molecules are drawn using van der Waals radii to the same scale. Hexagonal and pentagonal faces are not regular polygons. Notice that the opening between water molecules is smaller than the size of N_2, CO_2, and CH_4 molecules.

Table 1b. Physical Properties of CH_4 and CO_2 Hydrate, Pure CO_2 and Water Relevant to CH_4 Replacement by CO_2 in Hydrate-Bearing Sediments: Thermal Properties[a]

Property	CH_4 Hydrate (sI)	CO_2 Hydrate (sI)	CO_2 Liquid	H_2O Liquid
Heat capacity c (kJ kg^{-1} K^{-1})	2.031 [263 K] (1); 2.080 sI (2); 2.250 sI (3); 2.077 [270 K] (4)	No data found	2.280 [280 K,10 MPa] (highly variable) (5)	4.218 [273 K]; 4.192 [283 K] (1)
Thermal conductivity λ (W m^{-1} K^{-1})	0.68 [273 K] (1); 0.49 [263 K] (2)	0.49 [263 K] (2)	~0.13 [12.5 MPa, 270 K] (6)	0.56 [273 K]; 0.58 [283 K] (1)
Thermal diffusivity $\kappa = \lambda\rho^{-1}c^{-1}$ (m^2 s^{-1})	3.1×10^{-7} (7)	No data found	6.07×10^{-8} [b]	1.33×10^{-7} [273 K]; 1.38×10^{-7} [283 K] (1)
Heat or enthalpy of dissociation and formation H (kJ mol^{-1})	52.7–56.9 [273 K] (1); ~53 (independent of P-T) (8)	63.6–57.7 (±1.8) (at quadruple points) (8)	Does not apply	(water to ice) ~6 (1)

[a]Numbers in parentheses indicate sources as follows: 1, *Waite et al.* [2009]; 2, *Sloan and Koh* [2008]; 3, *Makogon* [1997]; 4, *Handa* [1986] and *Yoon et al.* [2003]; 5, *Span and Wagner* [1996]; 6, *Vesovic et al.* [1990]; 7, *Waite et al.* [2007]; 8, *Anderson* [2003, 2004].
[b]Computed value.

2.3. Mechanical Properties

[11] The viscosity of water is 1–2 orders of magnitude higher than the viscosity of liquid CO_2; this pronounced difference in viscosity will affect fluid invasion flow paths (Table 1c). Bulk densities are similar for hydrate and water, ordered as $\rho_{CH4hyd} < \rho_{H2O} < \rho_{CO2hyd}$. The density of liquid CO_2 may exceed that of water, $\rho_{CO2(l)} > \rho_{H2O}$ (e.g., at 273.15 K for pressures above 25 MPa); differences in fluid density contribute to buoyancy effects on fluid flow. Liquid CO_2 is heavier than water in deep sea locations, but remains lighter than water near the continental shelf.

[12] The volume of water V_w increases when hydrate forms: $V_{hyd} \sim 1.234\ V_w$ for CH_4 hydrate and $V_{hyd} \sim 1.279\ V_w$ for CO_2 hydrate. Such a large volumetric change within the pore space causes volumetric strains in the sediment during hydrate formation and promotes skeletal instability and contraction during dissociation [*Lee et al.*, 2010]. The shear stiffness of CH_4 hydrate is $G \approx 3.5$ GPa (a similar value is expected for CO_2 hydrate). Bulk moduli for liquid H_2O and CO_2 are lower than that of solid hydrates, and the bulk modulus of liquid CO_2 is 1 order of magnitude lower than that of water. Correspondingly, the P wave velocity is ~3 times slower in liquid CO_2 than in water. The addition of CO_2 in hydrate reservoirs could increase measured seismic wave velocities by forming additional hydrate, or it could lower the measured velocity by displacing pore water. The interpretation of seismic data gathered during CO_2 injection

Table 1c. Physical Properties of CH_4 and CO_2 Hydrate, Pure CO_2 and Water Relevant to CH_4 Replacement by CO_2 in Hydrate-Bearing Sediments: Mechanical Properties[a]

Property	CH_4 Hydrate (sI)	CO_2 Hydrate (sI)	CO_2 Liquid	H_2O Liquid
Viscosity μ (Pa s)	Does not apply	Does not apply	$(2–8) \times 10^{-5}$ [5–30 MPa, 318 K] (1)	~1.5×10^{-3} [293 K] (2)
Density ρ (kg m^{-3})	929 [263 K] (3); 940 (4); 910 [273 K] (3, 5)	1110–1090 (6) [30 MPa]; 1054 (7)	~938–800 kg m^{-3} [10 MPa, 280–300 K] (highly variable) (8)	999.9 [0.1 MPa, 273 K]; 1003 ± 1.5 [10 MPa, 280–300 K]; 1030 ± 2 [3.5% salinity; 10 MPa, 280 –300 K] (9)
Water volume expansion upon hydrate formation V_{hyd}/V_w	1.234[b] (n = 6; ρ_{CH4hyd} = 930 kg m^{-3}; 100% occupancy)	1.279[b] (n = 6; ρ_{CO2hyd} = 1100 kg m^{-3}; 100% occupancy)	Does not apply	$V_{ice}/V_w = 1.09$
Coefficient of thermal expansion α (K^{-1})	sI hydrate 7.7×10^{-5} [200 K] (4); 2.64×10^{-4} (10)	sI hydrate 7.7×10^{-5} [200 K] (4)	No data found	$2 \pm 0.3 \times 10^{-4}$ [50 MPa, 273.15–283.15 K] (11)
Bulk modulus (GPa)	7.2 [277 K] (12); ~9 [273 K] (10); 8.73 [273 K] (13)	No data found	0.338–0.124 GPa [10 MPa, 280–300 K][b]	2.1–2.3 GPa [10 MPa, 280–300 K][b]
Shear modulus (GPa)	3.2 [277 K] (12); 3.54 [273 K] (13)	No data found	0	0
Poisson ratio	0.32 [273 K] (13)	No data found	~0.5	~0.5
V_P (m s^{-1})	3775 [273 K] (13)	No data found	~600–400 m s^{-1} [10 MPa, 280–300 K] (8)	1450–1518 [10 MPa, 280–300 K] (14)
V_S (m s^{-1})	1954 [273 K] (13)	No data found	0	0

[a]Numbers in parentheses indicate sources as follows: 1, *Thomas and Adams* [1965]; 2, *Fenghour et al.* [1998] and *Netherton et al.* [1977]; 3, *Waite et al.* [2009]; 4, *Sloan and Koh* [2008]; 5, *Kiefte et al.* [1985]; 6, *Aya et al.* [1997]; 7, *Uchida et al.* [1999]; 8, *Span and Wagner* [1996]; 9, *Millero and Poisson* [1981]; 10, *Klapproth et al.* [2003]; 11, *Bradshaw and Schleicher* [1970]; 12, *Handa* [1986] and *Yoon et al.* [2003]; 13, *Helgerud et al.* [2009]; 14, *Belogol'skii et al.* [2002].
[b]Computed value.

Table 1d. Physical Properties of CH_4 and CO_2 Hydrate, Pure CO_2 and Water Relevant to CH_4 Replacement by CO_2 in Hydrate-Bearing Sediments: Electrical Properties[a]

Property	CH_4 Hydrate (sI)	CO_2 Hydrate (sI)	CO_2 Liquid	H_2O Liquid
Electrical conductivity ($S\ m^{-1}$)	0.01 (1)	No data found	$<10^{-2}$ at less than 3000 K (2)	depends on ionic concentration Seawater: ~5
Dielectric permittivity (frequency < 1 GHz)	~2.5 [273 K] (1)	No data found	1.0 to 1.5 from 1 to 20 MPa [308 K] (3)	79–80 [293 K] (4)

[a]Numbers in parentheses indicate sources as follows: 1, *Galashev et al.* [2006]; 2, *Tanaka et al.* [2008]; 3, *Goldfarb et al.* [1999] and *Obriot et al.* [1993]; 4, *Israelachvili* [1991].

must account for changes in both hydrate saturation and pore fluid composition.

2.4. Electrical Properties

[13] The permittivity of liquid water is determined by the orientational polarization of water molecules (Table 1d). The water dipole rotation is hindered in hydrates. In addition, CH_4 and CO_2 are nonpolar molecules and do not contribute to orientational polarization. Hence, gas hydrates have much lower permittivity compared to liquid water [*Galashev et al.*, 2006]. The electrical conductivity of water increases almost linearly with ionic concentration at low salt concentration and it is much higher than the electrical conductivity of hydrates. The electrical conductivity of liquid CO_2 is even lower than the electrical conductivity of hydrate. As with seismic surveys, resistivity surveys must account for pore fluid changes as well as hydrate saturation changes. In contrast to seismic results, in which added hydrate formation and CO_2 displacement of pure water have opposing effects on the measured velocity, the electrical properties are reduced both by added hydrate formation and pore water displacement. Tracking hydrate saturation and pore water chemistry is essential for correctly interpreting electrically based monitoring techniques.

2.5. Chemical Properties: Phase Boundaries, Solubilities, and Diffusivities

[14] Hydrate stability and gas solubility in water are pressure and temperature dependent (Tables 2, 3, and 4).

2.5.1. Phase Boundaries

[15] We develop regression equations for CO_2 and CH_4 hydrate phase boundaries, and for the liquid-vapor (L-V) boundary for CO_2 by fitting values predicted using experimentally validated thermodynamic models by *Duan and Sun* [2003] and *Sun and Duan* [2005] (Table 2). Hydrate grown from a mixed CH_4-CO_2 gas atmosphere exhibits an intermediate phase boundary, between the boundary for pure CH_4 and CO_2 hydrates, where the relative position scales with the mixture ratio [*Adisasmito et al.*, 1991; *Seo and Lee*, 2001]. The L-V boundary shown in Figure 2 corresponds to pure CO_2. Even small amounts of CH_4 in CO_2 cause the gas mixture L-V boundary to shift toward higher pressures, e.g., CO_2 with 10% CH_4 condenses at a pressure ~2 MPa higher than the pressure needed for pure CO_2 [*Donnelly and Katz*, 1954]. It can be observed from Figure 2 that: CH_4 hydrate stability requires higher pressures than CO_2 hydrate for temperatures $T \leq 283.67$ K. These boundaries partition the P-T space into four regions: CH_4 hydrate may be surrounded by liquid CO_2 (zone A) or by gaseous CO_2 (zone B) if $T < 277.1$ K; CO_2 hydrate can coexist with either liquid CO_2 (zone C) or with gaseous CO_2 (zone D).

2.5.2. Solubility in Liquid Phases

[16] Table 3 shows a summary of solubility values for all participating species in different media; the simultaneous presence of CH_4 and CO_2 in water alters the solubilities shown for simple binary systems [*Qin et al.*, 2008]. The solubility of CH_4 and CO_2 in water affects gas transport, hydrate formation and hydrate dissolution in water that is not fully saturated with gas. The solubility of CO_2 in water is about 10 times greater than that of CH_4; both solubilities increase as pressure increases and temperature decreases. The presence of hydrate in water inverts these trends. The amount of dissolved water in liquid CO_2 is not negligible, and can be as high as 0.003–0.006 mol mol^{-1}, that is ~1 kg of water per m^3 of liquid CO_2 at $T = 285$–293 K and $P = 10$–20 MPa [*Spycher et al.*, 2003]. Hence, liquid CO_2 can remove water, effectively "drying" the sediment.

Table 2. Phase Boundaries for Pure CH_4 and CO_2 Hydrates, and Liquid-Vapor Boundary for Pure CO_2, Calculated by Fitting Values Predicted Using the Experimentally Validated Formulation of *Duan and Sun* [2003] and *Sun and Duan* [2005][a]

CH_4 Hydrate Stability Boundary	CO_2 Hydrate Stability Boundary	CO_2 Liquid-Vapor Phase Boundary
Ice-hydrate-CH_4 gas; $P^* = 17.126T^* - 14.584$, if $263 < T \leq 273.15$ K	Ice-hydrate-CO_2 gas; $P^* = 8.082\ T^* - 7.020$; if $263 < T \leq 272.15$ K	$P^* = 3.45\ (T^*)^{7.00}$ if $263\ \text{K} < T \leq T_{critical} = 304.1$ K (note that boundary shifts to higher pressures in CH_4/CO_2 gas mixtures)[b]
Liquid water-hydrate-CH_4 gas; $T^* = 0.0396\ e^{(-0.000646\ P^*)}$ [24.348 + ln (P^*)] if $273.15 < T < 290$ K	Liquid water-hydrate-CO_2 gas; $T^* = 0.0358\ e^{(-0.00285\ P^*)}$ [27.829 + ln (P*)] if $272.15 < T \leq 283.17$ K Liquid water-hydrate-CO_2 liquid; $P^* = 3.34 \times 10^{-4}\ (T^*)^{264.4}$ if $283.17 < T < 290$ K	

[a]Definitions $P^* = P/1$ MPa; $T^* = T/273.15$ K.
[b]*Donnelly and Katz* [1954].

Table 3. Mutual Solubilities in Binary Mixtures for Liquid and Gaseous Media[a]

Rich Phase Medium	Solute	Concentration (mol kg^{-1})		
		3 MPa, 273 K	6.6 MPa, 274 K	10 MPa, 285 K
		Liquid Medium		
H_2O (without hydrate)	CH_4	0.11[b]	0.12[b]	0.13[b]
	CO_2	1.39[b] [~0.025 mol mol^{-1}]	1.66[b] [~0.030 mol mol^{-1}]	1.72
H_2O (with hydrate)	CH_4	0.060	0.063	0.116
	CO_2	0.89 [0.016 mol mol^{-1}]	0.83 [0.015 mol mol^{-1}]	Outside HSZ
CO_2	H_2O	Does not apply (Gas CO_2)	0.050[c] [2.2×10^{-3} mol mol^{-1}]	0.056 [2.5×10^{-3} mol mol^{-1}]
	CH_4	Does not apply (Gas CO_2)	Bubble point for 12% molar CH_4/CO_2 mixture	Supercritical mixture
		Gas Medium		
CH_4	H_2O	0.016 [~2.5×10^{-4} mol mol^{-1}]	0.008 [1.34×10^{-4} mol mol^{-1}]	0.012 [2.0×10^{-4} mol mol^{-1}]
CO_2	H_2O	0.011[~5×10^{-4} mol mol^{-1}]	Does not apply (Liquid CO_2)	Does not apply (Liquid CO_2)
CO_2	CH_4	Gas mixture	Does not apply (Liquid CO_2)	Does not apply (Liquid CO_2)

[a]Sources are *Donnelly and Katz* [1954], *Duan and Sun* [2003], *Folas et al.* [2007], *Hashemi et al.* [2006], *Spycher et al.* [2003], and *Sun and Duan* [2007].
[b]These values are extrapolations of solubility without hydrate to lower temperatures.
[c]Value for 285 K.

[17] Similarly, CH_4 is highly soluble in liquid CO_2; for example, a molar mixture of 12% CH_4 and 88% CO_2 remains liquid above a line defined between [6.6 MPa, 273.1 K] and [7.2 MPa, 278.1 K], as can be estimated from the bubble point line [*Donnelly and Katz*, 1954]. This observation explains experimental results at 8.7 MPa and 277.1 K where no CH_4 bubbles were observed during CH_4-CO_2 replacement (~2/40 mol of CH_4 per mol of CO_2) [*Dunk et al.*, 2006] as the liquid CO_2 was able to contain CH_4 molecules in solution preventing the formation of a separate phase. Finally, we observe that, the mixture CH_4-CO_2 has remarkably different bubble point and dew point lines as function of the molar ratio between CH_4 and CO_2 [see *Austegard et al.*, 2006; *Donnelly and Katz*, 1954; *Mraw et al.*, 1978]. As a result, gaseous CO_2 and CH_4 will coexist in equilibrium with liquid CO_2 and CH_4 in a fairly large pressure interval.

2.5.3. Water Vapor Concentration in Gaseous Phase

[18] Water evaporates into gaseous atmospheres (Table 3). For example, 0.016 kg of H_2O can be found per cubic meter of CO_2 gas at 3 MPa-273 K (0.011 mol H_2O per kg of CO_2) [*Spycher et al.*, 2003], and 0.005 kg of H_2O can be found per cubic meter of CH_4 gas at 3 MPa-273 K (0.012 mol H_2O per kg of CH_4) [*Folas et al.*, 2007]. We have consistently observed in separate experimental systems that water vapor in either CO_2 or CH_4 atmospheres can crystallize on hydrate surfaces promoting hydrate growth in relatively short time scale (days).

2.5.4. Mutual Diffusivities

[19] Diffusion controls most long-term phenomena, including hydrate formation and CH_4-CO_2 replacement [*Davies et al.*, 2008; *Svandal et al.*, 2006] (Table 4). The diffusivities of CO_2 and CH_4 in water are about the same, however, the diffusivity of H_2O in liquid CO_2 is up to 2 orders of magnitude higher [*Espinoza and Santamarina*, 2010]. High water diffusivity and solubility in liquid CO_2 make liquid and supercritical CO_2 an effective water-drying fluid agent.

[20] The diffusivity of CO_2, CH_4 or H_2O molecules through the solid hydrate mass is much slower than through liquids (note that preferential diffusive transport is expected along crystal imperfections and along the adsorbed water layer between hydrate and minerals). Therefore, CO_2 or CH_4 transport through solid hydrate will be much slower than through water. If the CH_4-CO_2 replacement is limited by diffusive transport, laboratory experiments and field implementations must seek to increase the surface contact area.

3. Previous Studies: Rates of Reaction

[21] Previous CH_4-CO_2 replacement studies documented in the literature are summarized in Table 5 and P-T conditions are plotted on Figure 2. As noted in Table 5, we describe the time-dependent replacement of CH_4 by CO_2 using the replacement ratio in the hydrate: $CO_2/(CH_4+CO_2) = A(1\text{-}e^{-t/\alpha})$, with A being the maximum replacement ratio at

Table 4. Mutual Diffusivities in Binary Water-CO_2 and Water-CH_4 Systems

Rich Phase Medium[a]	Diffusing Substance	Diffusivity (m^2 s^{-1})	Pressure (MPa)	Temperature (K)	Method	Reference
			Liquid			
H_2O	CO_2	1.37×10^{-9} to 1.64×10^{-9}	0.1	291.5–298	Experimental	*Thomas and Adams* [1965]
	CH_4	0.85×10^{-9} to 1.49×10^{-9}	0.1	277–293	Experimental	*Witherspoon and Bonoli* [1969]
CO_2	H_2O	6×10^{-8} to 18×10^{-8}	7–15	298	Experimental	*Espinoza and Santamarina* [2010]
H_2O (I)	CO_2	0.9×10^{-10}	No data	270	Molecular dynamics	*Ikeda-Fukazawa et al.* [2004]
H_2O (I)	CH_4	1.0×10^{-10}	No Data	270	Molecular dynamics	*Ikeda-Fukazawa et al.* [2004]
			Solid			
CH_4 (H)	CH_4	3.4×10^{-13} to 7.6×10^{-13}	3–15	263–268	Experimental	*Davies et al.* [2008]
CO_2 (H)	CO_2	1.0×10^{-12}	No data	273	Molecular dynamics	*Demurov et al.* [2002]
CO_2 (H)	H_2O	1.0×10^{-23}	No data	200	Molecular dynamics	*Demurov et al.* [2002]

[a]I, ice; and H, hydrate.

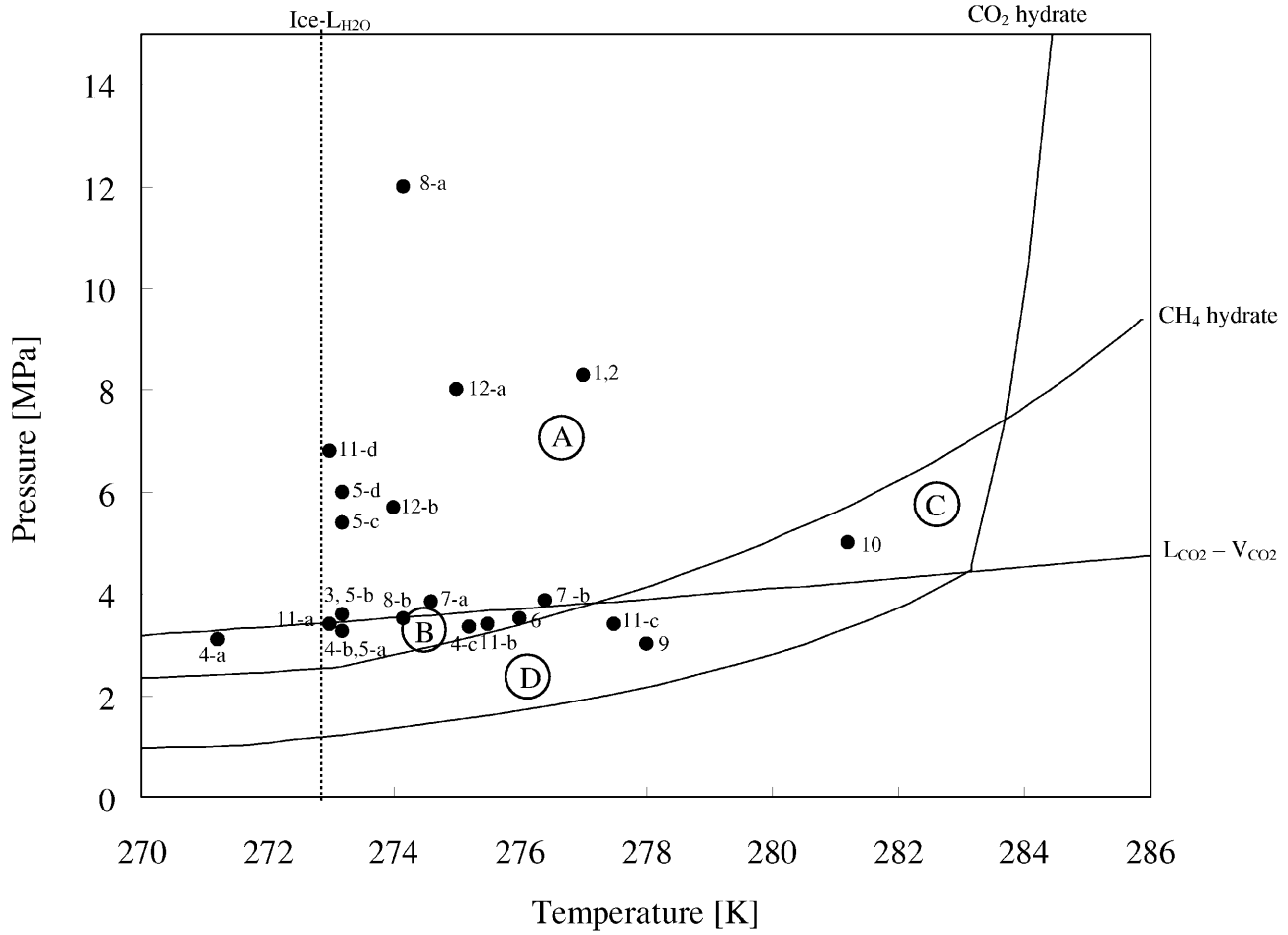

Figure 2. Dissociation phase boundaries for CO_2 and CH_4 hydrates, liquid-vapor phase boundary for pure CO_2, and liquid water-ice boundary. Data points show fluid pressure and temperature conditions for CH_4-CO_2 replacement studies reported in the literature (numbers correspond to tests listed in Table 5). Notice that CO_2 and CH_4 hydrate phase boundaries cross at ~7.5 MPa and 283.7 K. Furthermore, the CO_2 liquid-vapor boundary intersects the two dissociation lines creating four different zones inside the CO_2 hydrate stability field, above the liquid water-ice boundary.

long times, t. We obtain both A and the characteristic time, α, by fitting the published reaction time data. The following preliminary observations can be made from these studies: (1) hydrate replacement rates increase near the CH_4 hydrate phase boundary (data of *Ota et al.* [2005a], also mentioned by *McGrail et al.* [2007]), and (2) the reaction rate increases with increasing CO_2 gas pressure, eventually becoming constant when CO_2 liquefies (data of *Ota et al.* [2007]). We can also anticipate that high specific surface CH_4 hydrate experiences relatively fast replacement rates (refer to *Kim et al.* [1987]). There is some supportive evidence in the listed studies, but they are not conclusive due to lack of experimental details.

4. New Pore Scale Experimental Studies

[22] Multiple coexisting processes take place during CH_4-CO_2 replacement, including heat release, dissolution of participating species into different phases, volume change and mass transport. The following two experimental studies document these pore-scale processes. Figure 3 shows the experimental devices and P-T trajectories. Both experiments are monitored using time-lapse photography. We use digital image processing to estimate length and volume information (resolution: 1 pixel~10 μm), and we infer mass changes from measured volumes and the known density of the phases.

4.1. Water Droplet

[23] A water droplet (initial mass 36.1 mg) rests on a hydrophobic PTFE substrate and forms a quasi-semi-spherical body (~2.5 mm radius). Air is evacuated from the chamber by imposing a partial vacuum, followed by CH_4 pressurization (P = 5.9 MPa, T = 293 K, Figure 3b) and subsequent cooling. Some water evaporates into the methane atmosphere; we predict a ~1.2 mg water mass loss from the droplet (based on gas medium solubility information in Table 3). Given a water density of ~1000 kg m^{-3} (Table 1c), this agrees with the volume reduction we measured after 5 days (±0.1 mg precision). The first hydrate formation event follows transient ice formation. Later, we dissociate

Table 5. Previous CH_4-CO_2 Replacement Studies[a]

Test	P (MPa)	T (K)	CH_4 Hydrate Formation Method	Medium	Duration (h)	Replacement Ratio A[b]	Characteristic Time α[b] (h)	Monitoring	Reference
1	8.3	277	-	Sandstone	300	0.64	128	MRI	*Husebo et al.* [2008]
2	8.3	277	-	Sandstone	350	-	-	MRI	*Stevens et al.* [2008]
3	3.6	273.2	Stirring	No sediment	300	0.34	85	Raman spectroscopy	*Ota et al.* [2005b]
4-a	3.10	271.2	Stirring	No sediment	150	0.16	48	Raman spectroscopy	*Ota et al.* [2005a]
4-b	3.26	273.2	Stirring	No sediment	150	0.16	42	Raman spectroscopy	*Ota et al.* [2005a]
4-c	3.34	275.2	Stirring	No sediment	150	0.21	39	Raman spectroscopy	*Ota et al.* [2005a]
5-a	3.26	273.2	Stirring	No sediment	300	0.26	98	Raman spectroscopy	*Ota et al.* [2007]
5-b	3.6	273.2	Stirring	No sediment	300	0.34	94	Raman spectroscopy	*Ota et al.* [2007]
5-c	5.4	273.2	Stirring	No sediment	300	0.17	94[c]	Raman spectroscopy	*Ota et al.* [2007]
5-d	6.0	273.2	Stirring	No sediment	300	0.31	94[c]	Raman spectroscopy	*Ota et al.* [2007]
6	3.5	276	Powder ice: 100 μm	No sediment	12	0.92	1.0	Raman spectroscopy	*Komai et al.* [2000]
7-a	3.85	274.6	Stirring	No sediment	800	0.55	222	Water and gas produced	*Hirohama et al.* [1996]
7-b	3.88	276.4	Stirring	No sediment	800	0.64	329	Water and gas produced	*Hirohama et al.* [1996]
8-a	12.0	274.15	Powder ice: 5–50 μm	No sediment	30	0.92	4.2	NMR	*Park et al.* [2006]
8-b	3.5	274.15	Powder ice: 5–50 μm	No sediment	30	0.85	5.2	NMR	*Park et al.* [2006]
9	3.0	278	Powder ice: 100–250 μm	No sediment	150	1.00	22	Raman spectroscopy	*Yoon et al.* [2004]
10	5.0	281.2	-	Quartz sand	100	0.19	33 (L-CO_2)	Gas produced	*Zhou et al.* [2008b][d]
			-	Quartz sand		0.27	31 (90% emulsion)	Gas produced	*Zhou et al.* [2008b][d]
			-	Quartz sand		0.26	29 (70% emulsion)	Gas produced	*Zhou et al.* [2008b][d]
			-	Quartz sand		0.24	26 (30% emulsion)	Gas produced	*Zhou et al.* [2008b][d]
11-a	3.4	273	Stirring	No sediment	11	No data	No data	Raman spectroscopy	*McGrail et al.* [2007]
11-b	3.4	275.5	Stirring	No sediment	11	No data	No data	Raman spectroscopy	*McGrail et al.* [2007]
11-c	3.4	277.5	Stirring	No sediment	11	No data	No data	Raman spectroscopy	*McGrail et al.* [2007]
11-d	6.8	300–273	-	Sand	1.7	No data	No data	Raman spectroscopy	*McGrail et al.* [2007]
12-a	8.0	275.0	See section 4	No sediment	-	No data	No data	Time-lapse photography	This study
12-b	7.2	274.0	See section 4	No sediment	-	No data	No data	Time-lapse photography	This study

[a]Cases are plotted in Figure 2 using the same test numbers listed here.
[b]Replacement ratio = $A(1\text{-}e^{-t/\alpha})$, A, final replacement ratio; α, replacement rate.
[c]Limited data available.
[d]Ill-defined test.

this CH_4 hydrate by heating (not shown in Figure 3b), and we cool the sample back into the CH_4 hydrate stability field. CH_4 hydrate nucleates again in the form of a hydrate film that grows at the water-gas interface and propagates along the interface at a velocity of ~0.02 mm s^{-1}, forming a complete hydrate shell in less than 5 min (data shown in the auxiliary material).[1] For this growth velocity, heat transfer models predict a hydrate film thickness greater than 40 μm [*Mochizuki and Mori*, 2006]. We estimate the initial film thickness is equal to ~60 μm based on the droplet volume expansion $V_{final}/V_{initial}$ = 1.016 and the theoretical volume change from water to hydrate V_{hyd}/V_w = 1.234 (Table 1c). Stable P-T conditions are maintained for ~2 days; during this period, further hydrate growth is controlled by CH_4 diffusion through the hydrate layer (Figure 4a). The shell remains stable (note that shell depressions were observed in hydrate-coated droplet experiments by *Servio and Englezos* [2003]).

[24] We flood the chamber with liquid CO_2, displacing CH_4 gas through a vent (Figure 4b); the pressure and temperature conditions are inside the CH_4 hydrate stability field (P = 7±1 MPa, T = 275±1.5 K during the short injection period). The amount of water needed to saturate the liquid CO_2 in the absence of any hydrate in the chamber is ~45 mg (based on solubility data for a liquid medium in Table 3). We measure ~15 mg of water migration from the droplet to the surrounding liquid CO_2 in a period of 2 days; this is a form of "drying" in a CO_2 atmosphere (Figure 4). Thereafter, the droplet size remains constant for ~4 days under stable P-T conditions (P = 6 MPa, T = 274 ± 1 K; Figure 4i). These measurements suggest a lower solubility of water in CO_2 in the presence of hydrate than the value reported in the absence of hydrate (similarly to gas solubility in water, Table 3). While we assume replacement is taking place, no CH_4 gas bubbles form in the liquid CO_2 due to the high solubility of CH_4 in CO_2 (Table 3). We depressurize the chamber gradually. The hydrate shell remains stable after CO_2 vaporizes and also across the CH_4 hydrate phase boundary. We hold stable P-T conditions above the CO_2 hydrate boundary for ~30 min. Finally, we depressurize the chamber further and hydrate dissociates across the CO_2 hydrate phase boundary at ~1.8 MPa and 276.5 K.

4.2. Water Meniscus

[25] In this second study, the water droplet rests between two water-wet hydrophilic transparent glass surfaces, creating a cylindrically shaped body of water similar to a water

[1]Auxiliary materials are available in the HTML. doi:10.1029/2009JB000812.

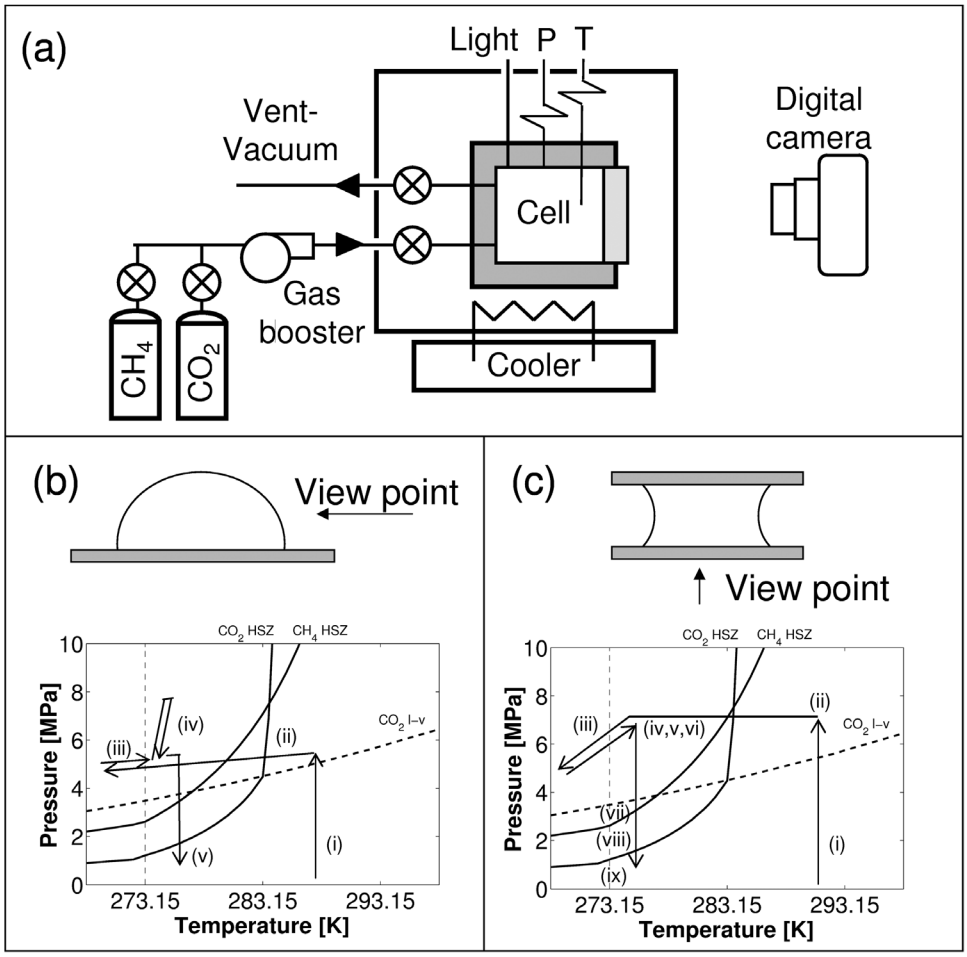

Figure 3. Experimental studies. (a) Pressure cell and devices. (b) Droplet experiments: path i, CH_4 pressurization; path ii, cooling; path iii, CH_4 hydrate formation; path iv, liquid CO_2 injection; and path v, CH_4-CO_2 hydrate dissociation. (c) Meniscus experiments: path i, CH_4 pressurization; path ii, cooling; path iii, ice formation; path iv, ice melting; path v, CH_4 hydrate formation; path vi, injection of liquid CO_2; path vii, liquid CO_2 to gas; path viii, exit CH_4 hydrate stability field; and path ix, exit CO_2 hydrate stability field. Both experiments are conducted using deionized water and research purity gases.

meniscus between two grains (8.7 mm diameter, 1.97 mm in height; and 120 mg water mass). Figure 3c shows the P-T trajectory imposed during the test. The evolution of the droplet is observed through the lower plate (Figure 5a). We trigger nucleation by causing transient ice formation (Figure 5b). Methane hydrate starts forming at the interface (similar to observation by *Stern et al.* [1998]). Hydrate does not grow homogeneously but advances in the form of lobes that invade the water meniscus (Figures 5c and 5d; needle-type growth is observed in the results reported by *Subramanian and Sloan* [2002]). Volume expansion during hydrate growth ($V_{hyd}/V_w = 1.234$, Table 1c) causes water to flow out of the meniscus along the hydrophilic glass surfaces, readily forming a thin hydrate layer on the glass plates (Figures 5c, 5d, and 5e). The hydrate growth rate inside the meniscus is between 0.05 and 0.11 mm h^{-1}. This fast growth rate suggests that gas reaches the water through cracks in the hydrate shell rather than by diffusion through the hydrate layer.

[26] The injection of liquid CO_2 is expected to trigger CH_4-CO_2 replacement and water dissolution into the liquid CO_2 (the amount of water needed to saturate the liquid CO_2 in this chamber is 171 mg, Table 3). Hence, the CO_2 hydrate film observed coating the glass plates in Figure 5f appears to be thinner (i.e., more transparent) than the CH_4 hydrate film in Figures 5d and 5e. Once again, CH_4 gas bubbles are not observed. The lobular hydrate structure remains inside the meniscus, that is, the overall geometry of the solid hydrate mass is preserved. Depressurization from liquid CO_2 to gaseous CO_2 causes the water dissolved in liquid CO_2 to precipitate as CO_2 hydrate on the glass plate (Figure 5g). Depressurization out of the CH_4 phase boundary has no "observable" effect on the hydrate phase within the meniscus or coating the glass surfaces (Figure 5h). Finally, hydrate dissociates during depressurization below the CO_2 hydrate phase boundary.

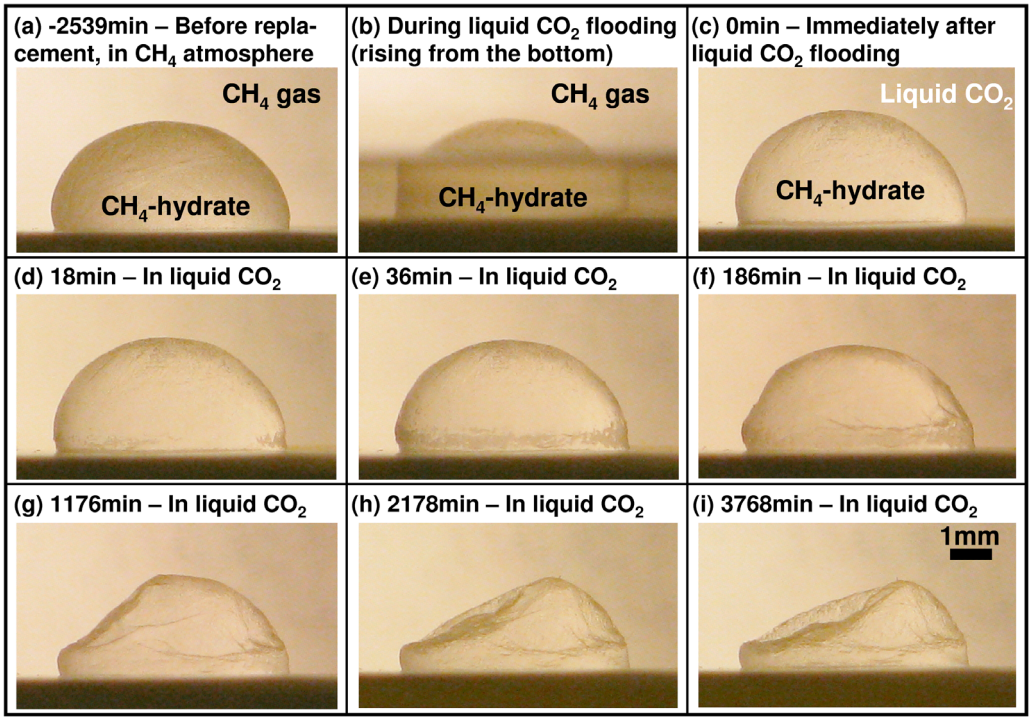

Figure 4. Droplet experiment: time evolution of the CH_4 hydrate shell after flooding with liquid CO_2. Pressure is 6 MPa, and the chamber temperature stays at 274 ± 1 K, after point iv in Figure 3b. This sequence of images suggests that liquid CO_2 "dries" the water either in the hydrate shell and/or inside the hydrate droplet.

4.3. Summary

[27] These two experiments reveal marked differences in CH_4 hydrate formation behavior on hydrophilic and hydrophobic substrates, and show the significance of mutual solubilities during CH_4-CO_2 replacement. There is no visual evidence of CH_4-CO_2 replacement when the CH_4 atmo-

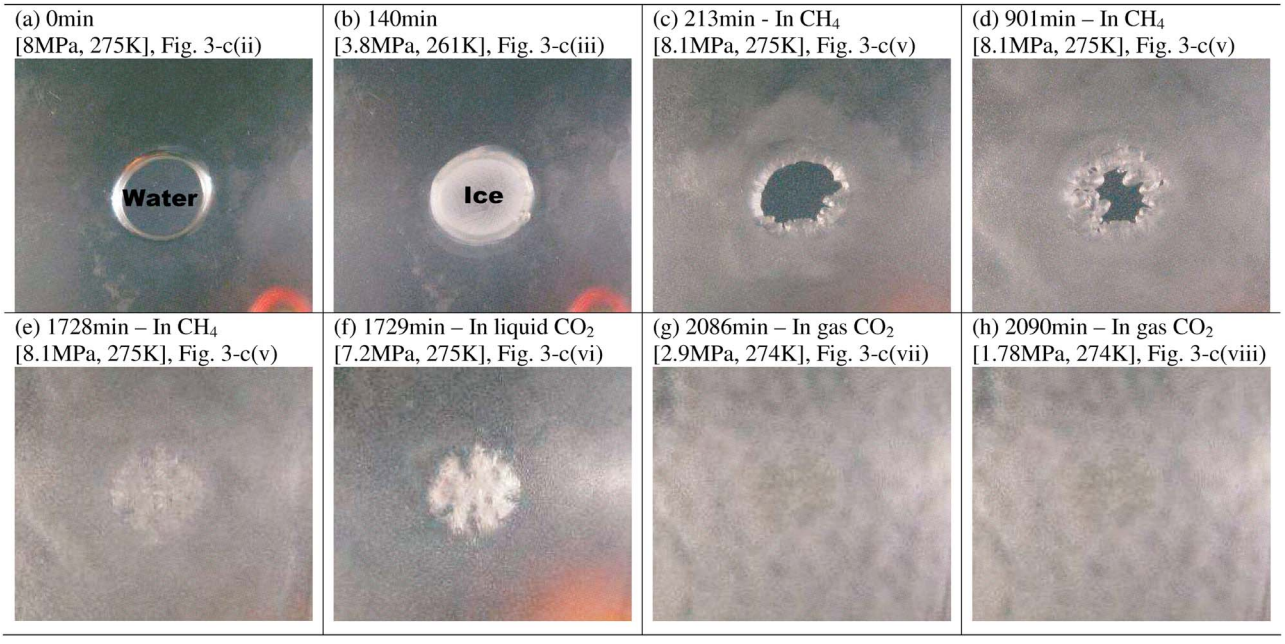

Figure 5. Meniscus experiment. (a) Water droplet, scale 8.7 mm diameter, (b) ice formation, (c–e) CH_4 hydrate formation and growth, (f) injection of liquid CO_2, (g) depressurization from liquid CO_2 to gas CO_2, and (h) image for P-T conditions outside the CH_4 hydrate stability field.

sphere is changed for CO_2 gas or liquid, i.e., there is no bubbling, volume change or alterations in the solid phase. The final depressurization stage confirms the presence of CO_2 hydrate at the CO_2 hydrate dissociation boundary.

5. Analysis: Sediment Scale Implications

[28] Analyses and experimental results presented in sections 2–4 allow us to anticipate potential thermohydro-mechanical coupled processes during CH_4-CO_2 replacement in hydrate-bearing sediments.

5.1. Molecular Scale CH_4-CO_2 Replacement Process

[29] Molecular scale observations (section 2), diffusion rates (Tables 1 and 4), and experimental results (Table 5) point to a "local" solid-liquid-solid transition during CH_4-CO_2 replacement. Inside the stability field, CH_4 hydrate in equilibrium is constantly forming and breaking down at the interface, releasing and capturing CH_4 molecules (see molecular dynamics insight by *Báez and Clancy* [1994], *Báez and Clancy* [1995], and *Walsh et al.* [2009]). In a CO_2-rich medium, freed CH_4 molecules may be replaced by CO_2 molecules, forming CO_2 hydrate and releasing excess heat. This released heat causes a positive feedback by locally raising the temperature of neighboring hydrate cages toward the CH_4 hydrate phase boundary to facilitate the atomic-scale solid-liquid-solid CH_4-CO_2 replacement in a form of "chain reaction."

[30] This hypothetical replacement process allows us to identify two end-member replacement scenarios. First, constant hydrate break down and formation make CH_4-CO_2 replacement possible within the CH_4 hydrate stability field (zone A in Figure 2); in this case, reaction rates will be strongly dependent on the contact area between CO_2 and CH_4 hydrate. Second, excess heat liberated in the CH_4-CO_2 replacement transformation may sustain a high solid-liquid-solid reaction rate; in this case we anticipate a lower reaction rate as P-T conditions are further inside the CH_4 hydrate stability field.

5.2. Bound for Excess Heat-Assisted Reaction Within the CH_4 Stability Field

[31] The second end-member is analyzed next, taking into consideration all the phases involved. We assume that local P-T conditions reach the CH_4 hydrate dissociation boundary driven by the excess heat liberated in the total reaction (section 2, Tables 1a–1d). How far inside the stability field can the hydrate-bearing sediment be to experience this excess heat-assisted reaction?

[32] Consider CH_4 hydrate at initial pressure P_o, temperature T_o and surrounded by CO_2 (liquid in zones A and C; and gas in zone B, Figure 2), water, and the mineral structure of the host sediment. Let us also assume that all hydrate cages undergo gas replacement so that the liberated heat is proportional to the difference between the heat of dissociation of CH_4 hydrate, H^d_{CH4hyd} [kJ kg^{-1}], and the heat of formation of CO_2 hydrate, H^f_{CO2hyd} [kJ kg^{-1}]. We consider isobaric conditions and 100% replacement to calculate the increase in temperature ΔT from the in situ condition T_0 to the temperature T_b on the CH_4 hydrate stability boundary corresponding to pressure P_0,

$$\begin{aligned}&\left(M_{CO_2}c_{CO_2}+M_{CH_4hyd}c_{CH_4hyd}+M_wc_w+M_mc_m\right)\,T_o\\&\quad=\left(M_{CH_4}c_{CH_4}+M_{CO_2hyd}c_{CO_2hyd}+M_wc_w+M_mc_m\right)\,T_b\\&\quad-\left(H^f_{CO_2hyd}M_{CO_2hyd}-H^d_{CH_4hyd}M_{CH_4hyd}\right)\end{aligned}\tag{1}$$

where subscripts for specific heat c and mass M, are m for mineral and w for water. In this analysis, we do not consider changes in P-T phase boundary conditions for gas mixtures (refer to section 2.5.1). All masses M convert to volume V through the corresponding bulk densities ρ, and partial volumes are related to the total sediment volume V_T through the sediment porosity ϕ, and the volumetric fractions of hydrate S_{hyd}, water S_w, and gas S_g (CH_4 gas or CO_2 gas/liquid) in the pore space,

$$\begin{aligned}&V_{hyd}=S_{hyd}\phi V_T,\quad V_w=S_w\phi V_T,\quad V_g=S_g\phi V_T,\\&V_m=(1-\phi)V_T\end{aligned}\tag{2}$$

where $S_{hyd}+S_w+S_g = 1$. A simple close form analytical expression is obtained assuming that the heat stored in CO_2 and CH_4, and hydrates is similar before and after replacement $\rho_{CO2}S_{CO2}\phi c_{CO2} + \rho_{CH4hyd}S_{hyd}\phi c_{CH4hyd} \approx \rho_{CH4}S_{CH4}\phi c_{CH4} + \rho_{CO2hyd}S_{hyd}\phi c_{CO2hyd}$. Then, the CH_4-CO_2 replacement rate within the sediment will be maximized if the initial temperature of the reservoir is equal or greater than

$$T_o=T_b(P_0)-\frac{\left(H^f_{CO_2hyd}\rho_{CO2hyd}-H^d_{CH_4hyd}\rho_{CH4hyd}\right)\,S_{hyd}\phi}{\rho_{CO_2}S_{CO_2}\phi c_{CO_2}+\rho_wS_w\phi c_w+\rho_{CH_4hyd}S_{hyd}\phi c_{CH_4hyd}+(1-\phi)\rho_mc_m}\tag{3}$$

Numerical results are presented in Figure 6 for a CH_4 hydrate volume fraction $S_{hyd} = 0.5$. This equation is a lower bound for the excess heat-assisted CH_4-CO_2 replacement, since we assume that the liberated heat warms up the whole sediment mixture. The upper bound corresponds to the CH_4-CO_2 replacement for pure hydrate (line on the upper left corner in Figure 6). Local heating during replacement is between these two bounds.

5.3. Hydrate Dissolution in Liquid CO_2

[33] Liquid CO_2 will draw water and methane from the CH_4 hydrate until it reaches the solubility limit of water in CO_2 y^{H2O}_{CO2} (section 2.5.2). The change in hydrate saturation in the sediment ΔS_{hyd} due to hydrate dissolution in liquid CO_2 is

$$\Delta S_{hyd}=(1-S_{hyd})\left(\frac{1}{y^{H2O}_{CO2}}\frac{\rho_{CH4hyd}}{\rho_{CO2}}\frac{n\cdot m_{H2O}}{m_{CH4}+n\cdot m_{H2O}}\frac{m_{CO2}}{m_{H2O}}+1\right)^{-1}\tag{4}$$

where m represents molar mass, n represents the stoichiometric ratio, and ρ_{CH4hyd} and ρ_{CO2} are the mass densities of CH_4 hydrate and liquid CO_2 at the prevailing P-T conditions. A change in hydrate saturation of ΔS_{hyd}~0.001 is

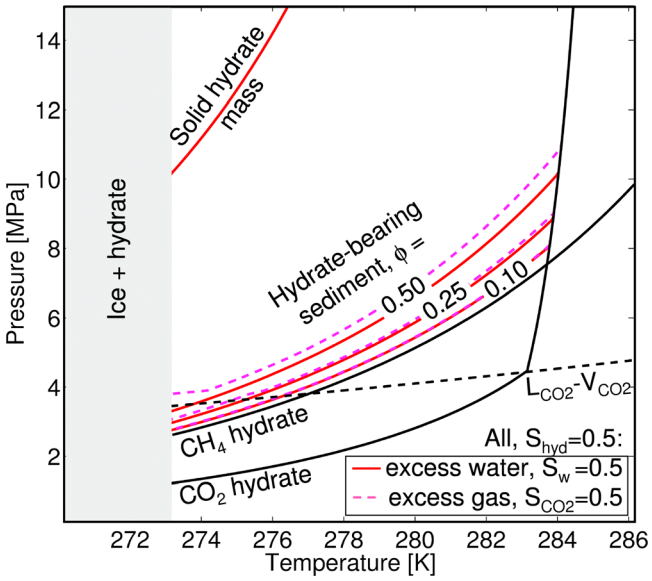

Figure 6. Pressure-temperature upper and lower bounds for initiating excess heat CH_4-CO_2 hydrate replacement by raising the local temperature to the CH_4 hydrate dissociation boundary. The temperature increases due to the heat released after CH_4 hydrate dissociation and CO_2 hydrate formation. At the upper bound, the reaction can begin far inside the CH_4 hydrate stability zone for a solid hydrate mass (upper bound ~10 K from the CH_4 hydrate dissociation boundary). At the lower bound, the reaction must begin closer to the CH_4 hydrate phase boundary in hydrate-bearing sediments where minerals and water absorb liberated heat. Bounds are computed using equation (3) and parameters from Table 1, porosity ϕ = 0.5, 0.25, 0.10; c_m = 0.83 kJ (kg K)$^{-1}$; H^f_{CO2hyd} = 395 kJ kg^{-1}; H^d_{CH4hyd} = 440 kJ kg^{-1}, ρ_{CO2hyd} = 1100 kg m^{-3}, and ρ_{CH4hyd} = 930 kg m^{-3}. Note that this analysis does not consider intermediate hydrate phase boundaries for hydrate grown from gas mixtures (section 2.5.1).

estimated for reservoir conditions $S_{hyd} < 0.3$, P = 5–8 MPa, and T = 273–278 K. While this is a small number, continuous flow of pure liquid CO_2, can cause significant hydrate dissolution, for instance near the CO_2 injection well.

5.4. Methane Gas Bubble Formation

[34] CH_4-CO_2 replacement releases CH_4 into the pore space. The critical CH_4 hydrate saturation S^*_{hyd} required to cause CH_4 bubble formation depends on the bubble point molar ratio R_{BP} for the CH_4-CO_2 fluid mixture at the specific P-T conditions. The value of S^*_{hyd} can be estimated as

$$S^*_{hyd} = (1 - S_w) \cdot \left(\frac{1}{R_{BP}} \frac{\rho_{CH4hyd}}{\rho_{CO2}} \frac{m_{CH4}}{m_{CH4} + n \cdot m_{H2O}} \frac{m_{CO2}}{m_{CH4}} + \frac{\rho_{CO2hyd}}{\rho_{CO2}} \frac{m_{CO2}}{m_{CO2} + n \cdot m_{H2O}} + 1 \right)^{-1} \quad (5)$$

For reservoir conditions P = 7.25 MPa and T = 278.15 K, the bubble point is R_{BP} = 0.12 [*Donnelly and Katz*, 1954], and the critical hydrate saturation for gas bubble formation is S^*_{hyd} ~0.21 (100% replacement is assumed, see Figure 7b).

5.5. Fluid Volume Expansion During CH_4-CO_2 Replacement

[35] Above bubbling conditions, CH_4-CO_2 replacement involves either volume change at constant fluid pressure, or pressure change under isochoric conditions. Let us compute first the change in volume during hydrate formation as a function of the hydration number n, mass densities ρ, and molar masses m

$$\frac{V_{hyd}}{V_w} = \frac{m_{hyd}/\rho_{hyd}}{m_w/\rho_w} = \frac{m_g + n \cdot m_w}{n \cdot m_w} \cdot \frac{\rho_w}{\rho_{hyd}} \quad (6)$$

where the density of water is ρ_w = 1000 kg m^{-3}, and molar masses are m_w = 18 g mol^{-1}, m_{CH4} = 16 g mol^{-1} and m_{CO2} = 44 g mol^{-1}. As shown in Figure 7a, an initial volume of water expands by V_{hyd}/V_w = 1.234 to form CH_4 hydrate (n = 6, ρ_{CH4hyd} = 930 kg m^{-3}), and V_{hyd}/V_w = 1.279 to form CO_2 hydrate (n = 6, ρ_{CO2hyd} = 1110 kg m^{-3}).

[36] The volume change of the hydrate mass during 100% CH_4-CO_2 replacement can be analyzed following a similar formulation and using experimentally measured macroscale quantities n and ρ (note that ρ is a function of n). Let us assume all CH_4 in hydrate exchanges with the injected liquid CO_2. The change in hydrate volume is

$$\frac{V_{CO2hyd}}{V_{CH4hyd}} = \frac{m_{CO2} + m_w \cdot n_{CO2}}{m_{CH4} + m_w \cdot n_{CH4}} \cdot \frac{\rho_{CH4hyd}}{\rho_{CO2hyd}} \quad (7)$$

The volume occupied by the hydrate mass expands about 1–6% after CH_4-CO_2 hydrate replacement (n_{CH4} = 6, n_{CO2} = 6, and pressure-dependent mass densities ρ_{CH4hyd} = 910–940 kg m^{-3}, ρ_{CO2hyd} = 1090–1110 kg m^{-3}). The change in lattice size ~2.9% is in agreement with this macroscale analysis (refer to values in Tables 1a–1d).

[37] On the other hand, released CH_4 gas after replacement occupies a volume that is strongly dependent on pressure and initial hydrate saturation. The final volume occupied by the released methane V_g^{CH4} which did not dissolve into the liquid CO_2, relative to the volume occupied by the CO_2 that became trapped in hydrate V_l^{CO2} is

$$\frac{V_g^{CH_4}}{V_l^{CO_2}} = \frac{\left[\frac{\rho_{CH4hyd}}{m_{CH4}} \frac{S_{hyd} \cdot m_{CH4}}{m_{CH4} + n \cdot m_{H2O}} - \frac{R_{BP}}{m_{CO2}} \left((1 - S_{hyd}) \rho_{CO2} - \frac{\rho_{CO2hyd} \cdot S_{hyd} \cdot m_{CO2}}{m_{CO2} + n \cdot m_{H2O}} \right) \right] \frac{m_{CH4}}{\rho_{CH4}}}{S_{hyd} \frac{\rho_{CO2hyd}}{\rho_{CO2}} \frac{m_{CO2}}{m_{CO2} + n \cdot m_{H2O}}} \quad (8)$$

There is a very pronounced increase in pore fluid volume associated with CH_4-CO_2 replacement at constant pressure. The volumetric ratio V_g^{CH4}/V_l^{CO2} is plotted in Figure 7b as a function of S_{hyd} for reservoir conditions P = 7.25 MPa, T = 278.15 K, R_{BP} = 0.12 [*Donnelly and Katz*, 1954]; for example, V_g^{CH4}/V_l^{CO2}~390% for S_{hyd} = 50%. Conversely, a marked increase in fluid pressure and decrease in effective stress will take place if constant volume is imposed during CH_4-CO_2 replacement. Field conditions will be between these two extreme scenarios. If replacement conditions result in a CH_4/CO_2 mixture, the volume of the mixture fluid

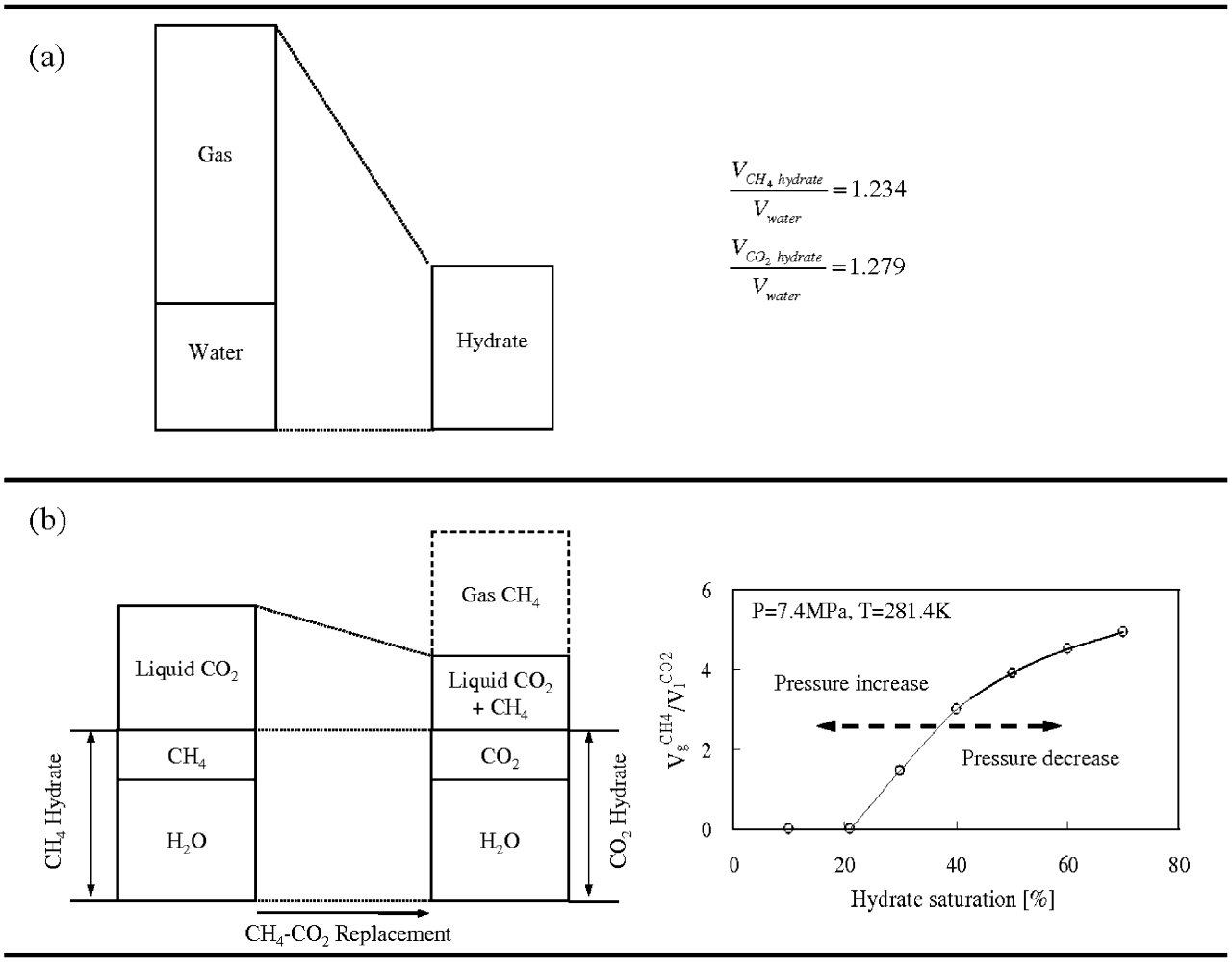

Figure 7. Volume change analysis. (a) During hydrate formation/dissociation, i.e., equation (7). (b) During CH_4-CO_2 replacement, i.e., equation (8) (P = 7.4 MPa, T = 281.4 K, ρ_{CO2} = 906 kg m^{-3}, bubble point for CH_4/CO_2 mixture R_{BP} = 12% mol CH_4/mol CO_2).

can be computed using cubic equations of state [*Li and Yan*, 2009].

5.6. Sediment Volume Change During CH_4-CO_2 Replacement

[38] A soil subjected to an increase in effective stress $\Delta\sigma'$ from an initial effective stress σ'_o to a final stress $\sigma'_o+\Delta\sigma'$ experiences a volumetric strain $\varepsilon_{vol} = C_c^*\log[(\sigma'_o+\Delta\sigma')/\sigma'_o]$ that is proportional to the compression index C_c^*. The presence of hydrates stiffens the soil skeleton so that lower values of the compression index are expected for hydrate-bearing sediments than for the same sediment without hydrates [*Lee et al.*, 2010]. The stiffening effect of hydrate depends on the pore habit: pore-filling (smallest effect), load-bearing and cementing (largest effect) [*Waite et al.*, 2009]. While CH_4-CO_2 replacement involves transient "local" dissociation, preliminary experimental evidence we have gathered using cementing CH_4 hydrate-bearing sands with hydrate saturation S_{hyd} = 5%–10% shows no significant change in global stiffness when wave propagation velocity data are gathered during CH_4-CO_2 gas replacement. Thus, low volumetric strains should be expected during CH_4-CO_2 replacement under free draining flow conditions. Fluid volume change may affect sediment stability if free draining conditions are lost during replacement. The following sequence of events may take place [*Santamarina and Jang*, 2009]: fluid volume expansion during the CH_4-CO_2 replacement causes an increase in fluid pressure, a decrease in effective stress, and a loss in sediment strength leading to shear failure, gas driven fractures, and/or collapse of the sediment skeleton.

5.7. Mixed Fluid Flow

[39] CO_2 is considerably less viscous than water, and CO_2 will tend to produce viscous fingering in excess-water reservoirs. Some recent numerical simulations show finger-like patterns when CO_2 invades water-saturated formations [*Kang et al.*, 2005; *Qi et al.*, 2009], while other simulations show minimal CO_2 fingering [*Chang et al.*, 1994]. The analysis of pore scale capillary and viscous forces suggests a higher tendency to viscous fingering in the near field of the injection well where flow velocities are high [*Lenormand et al.*, 1988].

Table 6. Anticipated Sediment Scale Phenomena During CH_4-CO_2 Gas Replacement[a]

	Reservoir Type	
Injected Fluid	Gas-Limited, Excess Water	Water-Limited, Excess Gas
Gas CO_2	Gas buoyancy affects invasion (1) Slow gas replacement rate due to low gas activity (3) Expect viscous fingering of CO_2 gas (5, 6)	CH_4 hydrate is found at contacts (2) Low hydrate volume expansion (1%–6%) (4) High CO_2 gas permeability CO_2 and CH_4 mix, and flow together (7)
Liquid CO_2	Released CH_4 gas lowers the mixture bulk modulus (if above bubble point concentration) (8) Large fluid volume expansion if released methane exceeds bubble point concentration (10) Expect viscous fingering of liquid CO_2 (5, 6)	Some of the water in CH_4 hydrate will dissolve into the liquid CO_2 and the final hydrate saturation will decrease; in fact, liquid CO_2 might "dry" hydrate near the injection well (9) Some CH_4 gas will remain trapped in the sediment
Either gas or liquid CO_2	Replacement rate is limited by spatial invasion of gas/liquid CO_2 At low injection rates or due to flow interruptions, CO_2 will react with the excess water to form hydrate during injection, plugging the formation and shielding CH_4 hydrate at reservoir and pore scales (3, 5) Hydrate saturation increases and hydraulic conductivity decreases (11) Water acidifies (12)	The sediment is water limited so it does not clog by forming new hydrate

[a]Numbers in parentheses are sources as follows: 1, *Lu et al.* [2009]; 2, *Waite et al.* [2009]; 3, *McGrail et al.* [2007]; 4, this study, equation (7); 5, *Kang et al.* [2005]; 6, *Lenormand et al.* [1988]; 7, *Donnelly and Katz* [1954]; 8, *Span and Wagner* [1996] and *Trusler and Zarari* [1992]; 9, this study, section 4, Figure 4; 10, this study, equation (8); 11, *Kleinberg et al.* [2003]; 12, *Kneafsey and Pruess* [2010].

5.8. Anticipated Sediment-Scale Emergent Phenomena

[40] Four different injection scenarios are identified in Table 6 in terms of P-T conditions that control either liquid CO_2 or gas CO_2 injection (zones A and B in Figure 2), and either excess-water (gas-limited) or excess-gas (water limited) hydrate-bearing sediments. Phenomena and properties listed above help us identify the following processes that may take place during injection:

[41] 1. The release of CH_4 above the bubble point leads to gas formation $S_g > 0$ and lowers the relative permeability of the liquid phase (van Genutchen's equation as in the work by *Kleinberg et al.* [2003]).

[42] 2. A low velocity of the invading CO_2 front, compared to the rate of CO_2 hydrate formation, will promote the growth of new CO_2 hydrate in excess-water reservoirs, occlude regions with CH_4 hydrate, prevent the direct contact of CH_4 hydrate with CO_2, and hinder CH_4-CO_2 replacement (see numerical simulation of CO_2 hydrate clogging of *Kang et al.* [2005]).

[43] 3. The replacement rate in both excess-gas and excess-water reservoirs will be controlled by the spatial distribution of CO_2 during injection and the replacement reaction rate.

[44] Clogging by CO_2 hydrate formation can be analyzed by comparing the velocity of the invading CO_2 advective front and the growth velocity of CO_2 hydrate at the water-CO_2 interface. The advection fluid velocity in pores v_A [m s^{-1}] = $q/(2\pi r H_r \phi)$ is determined by the injection flow rate q [m^3 s^{-1}], the distance from the well to the front r, the hydrate-bearing reservoir thickness H_r [m], and the sediment porosity ϕ. The velocity of diffusion-controlled growth of the hydrate plug in pores is approximately $v_D = D/\delta$, where D is the diffusion coefficient [m^2 s^{-1}] of CO_2 through hydrate and δ [m] the length of the hydrate plug. The ratio of these two velocities $v_D/v_A = 2\pi DrH\phi/(\delta q)$ determines whether hydrate clogging ($v_D/v_A >> 1.0$) or unconstrained advection ($v_D/v_A << 1.0$) will take place. For example, clogging is not anticipated in sandy sediments and sandstones near the injection well during continuous injection, (assuming $\delta \sim 10^{-4}$ m, i.e., the plug length is similar to the pore size). However, a stagnant CO_2 fluid front will promote hydrate formation and a differential pressure $p_{CO2}-p_w$ will be needed to break the CO_2 hydrate seal in order to continue injecting CO_2. Assuming cylindrical pore geometry, the additional CO_2 pressure is $p_{CO2}-p_w = 4\beta\delta/d$, where β is the hydrate-mineral bonding strength, d is the pore diameter and δ the plug thickness. For plugs $d \sim \delta$ and a bonding strength $\beta \sim 250$ kPa, the differential pressure to reinitiate pumping is $p_{CO2}-p_w \sim 1$ MPa.

[45] The complex interaction among coexisting processes may give rise to emergent bifurcation phenomena such as viscous fingering and gas-driven fractures. On the other hand, self-homogenizing effects may also arise; for example, CH_4 gas production during CO_2 injection will reduce the local permeability and hinder the formation of CO_2 fingers.

6. Conclusions

[46] The replacement of CH_4 by CO_2 in hydrate-bearing sediments involves multiple coexisting processes, such as mass and heat transport, heat liberation, dissolution, gas production, and fluid volume change.

[47] The CH_4 hydrate cage must separate to release the CH_4 molecule and trap the CO_2 molecule. This transient and local solid-liquid-solid transition within the stability field is assisted by the excess heat liberated during CH_4-CO_2 replacement and can extend as far as ~10 K inside the stability field. The presence of minerals, water, and excess gas can limit this self-sustaining reaction to within ~3 K of the CH_4 hydrate boundary. While available data are limited, experimental and theoretical considerations suggest that replacement rates increase near the CH_4 hydrate phase boundary, with increasing pore fluid pressure until the CO_2 liquefies, and, when CH_4 hydrate masses are small so the contact surface available for CO_2 exchange is high.

[48] New experimental results highlight the high solubility of water and CH_4 in liquid CO_2. Hydrate-forming water dissolves into liquid CO_2, so that lower hydrate saturation is expected after CH_4-CO_2 replacement in water-limited reservoirs. The transient in hydrate stiffness that should accompany local solid-liquid-solid CH_4-CO_2 replacement has a very small effect on macroscale skeleton stiffness and the sediment should experience low volumetric strains during CH_4-CO_2 replacement under drained conditions.

[49] Processes and properties reviewed in this study allow us to anticipate various reservoir scale phenomena during CH_4-CO_2 replacement, including potential decrease in water saturation, decrease in the liquid relative permeability, pronounced increase in fluid volume when a CH_4 gas phase is formed, CO_2 hydrate clogging when the velocity of the invading front is low and there is enough water to supersaturate the CO_2, and the possibility of CO_2 fingering leading to CH_4 hydrate occlusion within the reservoir. Excess-gas methane hydrate reservoirs should be more amenable to CH_4-CO_2 replacement because of high permeability to CO_2, large interface between CH_4 hydrate and CO_2, and no early CO_2 hydrate clogging. Volume-pressure changes associated to CH_4-CO_2 replacement in excess-water reservoirs may cause increase in fluid pressure, decrease in effective stress and strength loss, volume expansion, and gas-driven fractures if a CH_4 gas phase develops and the permeability is low enough to prevent pressure dissipation.

Notation

n stoichiometric ratio.
H heat energy [kJ mol^{-1}].
λ thermal conductivity [W m^{-1} K^{-1}].
ρ density [kg m^{-3}].
ϕ porosity.
V volume [m^3].
T temperature [K].
G shear stiffness [Pa].
P pressure [Pa].
M mass [g].
m molar mass [g mol^{-1}].
S volumetric fractions.
R gas constant [J (mol K)$^{-1}$].
c specific heat [J kg^{-1} K^{-1}].
σ' effective stress [Pa].
C_c^* compression index.
ε volumetric strain.
R_{BR} bubble point ratio [mol mol^{-1}].
y_{CO2}^{H2O} solubility of water in CO_2 [mol mol^{-1}].
v_A advection fluid velocity [m s^{-1}].
q flow rate [m^3 s^{-1}].
r distance to the center of the wellbore [m].
H_r hydrate reservoir thickness [m].
v_D diffusion front velocity [m s^{-1}].
δ hydrate plug length [m].

[50] **Acknowledgments.** Support for this research was provided by U.S. Department of Energy. Additional funding was provided by the Goizueta Foundation. We are grateful to Keith Hester, an additional anonymous reviewer for multiple comments and suggestions, and William F. Waite's detailed review and insightful comments greatly improved the clarity and depth of the study.

References

Adisasmito, S., R. J. Frank III, and E. D. Sloan Jr. (1991), Hydrates of carbon-dioxide and methane mixtures, *J. Chem. Eng. Data*, *36*(1), 68–71, doi:10.1021/je00001a020.

Anderson, G. K. (2003), Enthalpy of dissociation and hydration number of carbon dioxide hydrate from the Clapeyron equation, *J. Chem. Thermodyn.*, *35*(7), 1171–1183, doi:10.1016/S0021-9614(03)00093-4.

Anderson, G. K. (2004), Enthalpy of dissociation and hydration number of methane hydrate from the Clapeyron equation, *J. Chem. Thermodyn.*, *36*(12), 1119–1127, doi:10.1016/j.jct.2004.07.005.

Austegard, A., E. Solbraa, G. De Koeijer, and M. J. Mølnvik (2006), Thermodynamic models for calculating mutual solubilities in H_2O-CO_2-CH_4 mixtures, *Chem. Eng. Res. Des.*, *84*(9), 781–794, doi:10.1205/cherd05023.

Aya, I., K. Yamane, and H. Naria (1997), Solubility of CO_2 and density of CO_2 hydrate at 30 MPa, *Energy*, *22*(2–3), 263–271, doi:10.1016/S0360-5442(96)00093-X.

Báez, L. A., and P. Clancy (1994), Computer-simulation of the crystal-growth and dissolution of natural-gas hydrates, *Ann. N. Y. Acad. Sci.*, *715*, 177–186, doi:10.1111/j.1749-6632.1994.tb38833.x.

Báez, L. A., and P. Clancy (1995), The kinetics of crystal-growth and dissolution from the melt in Lennard-Jones systems, *J. Chem. Phys.*, *102*(20), 8138–8148, doi:10.1063/1.469225.

Belogol'skii, V. A., S. S. Sekoyan, L. M. Samorukova, V. I. Levtsov, and S. R. Stefanov (2002), Temperature and pressure dependence of the speed of sound in seawater, *Meas. Tech.*, *45*(8), 879–886, doi:10.1023/A:1021130814860.

Bradshaw, A., and K. E. Schleicher (1970), Direct measurement of thermal expansion of sea water under pressure, *Deep Sea Res.*, *17*(4), 691–698.

Chang, Y. B., M.T. Lim, G.A. Pope, K. Sepehrnoori (1994), CO_2 flow patterns under multiphase flow: Heterogeneous field-scale conditions, *SPE Reservoir Eng.*, *9*(3), 208–216, doi:10.2118/22654-PA.

Circone, S., S. H. Kirby, and L. A. Stern (2005), Direct measurement of methane hydrate composition along the hydrate equilibrium boundary, *J. Phys. Chem. B*, *109*(19), 9468–9475, doi:10.1021/jp0504874.

Collett, T. S. (2002), Energy resource potential of natural gas hydrates, *AAPG Bull.*, *86*(11), 1971–1992.

Davies, S. R., J. W. Lachance, E. D. Sloan, and C. A. Koh (2008), A novel approach to measuring methane diffusivity through a hydrate film using differential scanning calorimetry, paper presented at 6th International Conference on Gas Hydrates, Vancouver, B. C., Canada.

Demurov, A., R. Radhakrishnan, and B. L. Trout (2002), Computations of diffusivities in ice and CO_2 clathrate hydrate via molecular dynamics and Monte Carlo simulations, *J. Chem. Phys.*, *116*(2), 702–709, doi:10.1063/1.1425821.

Donnelly, H., and D. Katz (1954), Phase equilibria in the carbon dioxide-methane system, *Ind. Eng. Chem.*, *46*(3), 511–517, doi:10.1021/ie50531a036.

Duan, Z. H., and R. Sun (2003), An improved model calculating CO_2 solubility in pure water and aqueous NaCl solutions from 273 to 533 K and from 0 to 2000 bar, *Chem. Geol.*, *193*(3–4), 257–271, doi:10.1016/S0009-2541(02)00263-2.

Dunk, R. M., P. G. Brewer, E. T. Peltzer, P. M. Walz, K. C. Hester, and E. D. Sloan (2006), The exchange reaction between methane hydrate and carbon dioxide: An oceanic feasibility test, *Eos Trans. AGU*, *87*(52), Fall Meet. Suppl., Abstract MR43A-1070.

Espinoza, D. N., and J. C. Santamarina (2010), Water-CO_2-mineral systems: Interfacial tension, contact angle, and diffusion—Implications to CO_2 geological storage, *Water Resour. Res.*, *46*, W07537, doi:10.1029/2009WR008634.

Fenghour, A., W. A. Wakeham, and V. Vesovic (1998), The viscosity of carbon dioxide, *J. Phys. Chem. Ref. Data*, *27*(1), 31–44, doi:10.1063/1.556013.

Folas, G. K., E. W. Froyna, J. Lovland, G. M. Kontogeorgia, and E. Solbraa (2007), Data and prediction of water content of high pressure nitrogen, methane and natural gas, *Fluid Phase Equilib.*, *252*(1–2), 162–174, doi:10.1016/j.fluid.2006.12.018.

Galashev, A. E., V. N. Chukanov, A. N. Novruzov, and O. A. Novruzov (2006), Molecular-dynamic calculation of spectral characteristics of absorption of infrared radiation by (H2O)(j) and (CH4)(i)(H2O)(n) clusters, *High Temp.*, *44*(3), 364–372, doi:10.1007/s10740-006-0046-7.

Goldfarb, D. L., D. P. Fernández, and H. R. Corti (1999), Dielectric and volumetric properties of supercritical carbon dioxide(1) plus methanol (2) mixtures at 323.15 K, *Fluid Phase Equilib.*, *158–160*, 1011–1019, doi:10.1016/S0378-3812(99)00146-6.

Handa, Y. P. (1986), Compositions, enthalpies of dissociation, and heat-capacities in the range 85 to 270 K for clathrate hydrates of methane, ethane, and propane, and enthalpy of dissociation of isobutane hydrate, as determined by a heat-flow calorimeter, *J. Chem. Thermodyn.*, *18*(10), 915–921, doi:10.1016/0021-9614(86)90149-7.

Hashemi, S., A. Macchi, S. Bergeron, and P. Servio (2006), Prediction of methane and carbon dioxide solubility in water, *Fluid Phase Equilib.*, *246*(1–2), 131–136, doi:10.1016/j.fluid.2006.05.010.

Helgerud, M. B., W. F. Waite, S. H. Kirby, and A. Nur (2009), Elastic wave speeds and moduli in polycrystalline ice Ih, sI methane hydrate, and sII methane-ethane hydrate, *J. Geophys. Res.*, *114*, B02212, doi:10.1029/2008JB006132.

Hirohama, S., Y. Shimoyama, A. Wakabayashi, S. Tatsuta, and N. Nishida (1996), Conversion of CH_4-hydrate to CO_2-hydrate in liquid CO_2, *J. Chem. Eng. Jpn.*, *29*(6), 1014–1020, doi:10.1252/jcej.29.1014.

Husebo, J., et al. (2008), Experimental investigation of methane release from hydrate formation in sandstone through both hydrate dissociation and CO_2 sequestration, paper presented at 6th International Conference on Gas Hydrates, Vancouver, B. C., Canada.

Ikeda-Fukazawa, T., K. Kawamura, and T. Hondoh (2004), Mechanism of molecular diffusion in ice crystals, *Mol. Simul.*, *30*(13–15), 973–979, doi:10.1080/08927020410001709307.

Israelachvili, J. (1991), *Intermolecular and Surface Forces*, 2nd ed., Academic, London.

Kang, Q. J., I. N. Tsimpanogiannis, D. Zhang, and P. C. Lichtner (2005), Numerical modeling of pore-scale phenomena during CO2 sequestration in oceanic sediments, *Fuel Process. Technol.*, *86*(14–15), 1647–1665, doi:10.1016/j.fuproc.2005.02.001.

Kiefte, H., M. J. Clouter, and R. E. Gagnon (1985), Determination of acoustic velocities of clathrate hydrates by Brillouin spectroscopy, *J. Phys. Chem.*, *89*(14), 3103–3108, doi:10.1021/j100260a031.

Kim, H. C., P. R. Bishnoi, R. A. Heidemann, and S. S. H. Rizvi (1987), Kinetics of methane hydrate decomposition, *Chem. Eng. Sci.*, *42*(7), 1645–1653, doi:10.1016/0009-2509(87)80169-0.

Klapproth, A., E. Goreshnik, D. Staykova, H. Klein, and W. F. Kuhs (2003), Structural studies of gas hydrates, *Can. J. Phys.*, *81*(1–2), 503–518, doi:10.1139/p03-024.

Kleinberg, R. L., C. Flaum, D. D. Griffin, P. G. Brewer, G. E. Malby, E. T. Peltzer, and J. P. Yesinowski (2003), Deep sea NMR: Methane hydrate growth habit in porous media and its relationship to hydraulic permeability, deposit accumulation, and submarine slope stability, *J. Geophys. Res.*, *108*(B10), 2508, doi:10.1029/2003JB002389.

Kneafsey, T. J., and K. Pruess (2010), Laboratory flow experiments for visualizing carbon dioxide-induced, density-driven brine convection, *Transp. Porous Media*, *82*(1), 123–139, doi:10.1007/s11242-009-9482-2.

Komai, T., Y. Yamamoto, and K. Ohga (2000), Dynamics of reformation and replacement of CO_2 and CH_4 gas hydrates, *Ann. N. Y. Acad. Sci.*, *912*, 272–280, doi:10.1111/j.1749-6632.2000.tb06781.x.

Kvenvolden, K. A. (1988), Methane hydrate—A major reservoir of carbon in the shallow geosphere?, *Chem. Geol.*, *71*(1–3), 41–51, doi:10.1016/0009-2541(88)90104-0.

Lee, J. Y., J. C. Santamarina, and C. Ruppel (2010), Volume change associated with formation and dissociation of hydrate in sediment, *Geochem. Geophys. Geosyst.*, *11*, Q03007, doi:10.1029/2009GC002667.

Lenormand, R., E. Touboul, and C. Zarcone (1988), Numerical models and experiments on immiscible displacements in porous media, *J. Fluid Mech.*, *189*, 165–187, doi:10.1017/S0022112088000953.

Li, H., and J. Yan (2009), Evaluating cubic equations of state for calculation of vapor-liquid equilibrium of CO_2 and CO_2-mixtures for CO2 capture and storage processes, *Appl. Energy*, *86*(6), 826–836, doi:10.1016/j.apenergy.2008.05.018.

Lu, C., W. S. Han, S.-Y. Lee, B. J. McPherson, and P. C. Lichtner (2009), Effects of density and mutual solubility of a CO_2-brine system on CO_2 storage in geological formations: "Warm" vs. "cold" formations, *Adv. Water Resour.*, *32*(12), 1685–1702, doi:10.1016/j.advwatres.2009.07.008.

Makogon, Y. (1997), *Hydrates of Hydrocarbons*, 482 pp., PennWell Books, Tulsa, Okla.

McGrail, B. P., et al. (2007), Using carbon dioxide to enhance recovery of methane from gas hydrate reservoirs: Final summary report. *Rep. PNNL-17035*, Pac. Northwest Natl. Lab., Richland, Wash.

Milkov, A. V. (2004), Global estimates of hydrate-bound gas in marine sediments: How much is really out there?, *Earth Sci. Rev.*, *66*(3–4), 183–197, doi:10.1016/j.earscirev.2003.11.002.

Millero, F. J., and A. Poisson (1981), International one-atmosphere equation of state of seawater, *Deep Sea Res., Part A*, *28*(6), 625–629, doi:10.1016/0198-0149(81)90122-9.

Mochizuki, T., and Y. H. Mori (2006), Clathrate-hydrate film growth along water/hydrate-former phase boundaries—Numerical heat-transfer study, *J. Cryst. Growth*, *290*(2), 642–652, doi:10.1016/j.jcrysgro.2006.01.036.

Mori, Y. H., and T. Mochizuki (2000), Modeling of simultaneous heat and mass transfer to/from and across a hydrate film, *Ann. N. Y. Acad. Sci.*, *912*, 633–641, doi:10.1111/j.1749-6632.2000.tb06818.x.

Mraw, S. C., S.-C. Hwang, and R. Kobayashi (1978), Vapor-liquid-equilibrium of CH_4-CO_2 system at low-temperatures, *J. Chem. Eng. Data*, *23*(2), 135–139, doi:10.1021/je60077a014.

Netherton, R., et al. (1977), Viscosity of brine from Salton sea geothermal field, California, from 25°C to 90°C at 100 kPa, *Eos Trans. AGU*, *58*(12), 1248.

Obriot, J., J. Ge, T. K. Bose, and J.-M. St-Arnaud (1993), Determination of the density from simultaneous measurements of the refractive-index and the dielectric-constant of gaseous CH_4, SF_6 and CO_2, *Fluid Phase Equilib.*, *86*, 314–350, doi:10.1016/0378-3812(93)87183-2.

Ota, M., Y. Abe, M. Watanabe, R. L. Smith Jr., and H. Inomata (2005a) Methane recovery from methane hydrate using pressurized CO2, *Fluid Phase Equilib.*, *228–229*, 553–559, doi:10.1016/j.fluid.2004.10.002.

Ota, M., K. Morohashi, Y. Abe, M. Watanabe, R. Lee Smith Jr., and H. Inomata (2005b), Replacement of CH_4 in the hydrate by use of liquid CO_2, *Energy Convers. Manage.*, *46*(11–12), 1680–1691, doi:10.1016/j.enconman.2004.10.002.

Ota, M., T. Saito, T. Aida, M. Watanabe, Y. Sato, R. L. Smith Jr., and H. Inomata (2007), Macro and microscopic CH_4-CO_2 replacement in CH_4 hydrate under pressurized CO_2, *AIChE J.*, *53*(10), 2715–2721, doi:10.1002/aic.11294.

Park, Y., D.-Y. Kim, J.-W. Lee, D.-G. Huh, K.-P. Park, J. Lee, and H. Lee (2006), Sequestering carbon dioxide into complex structures of naturally occurring gas hydrates, *Proc. Natl. Acad. Sci. U. S. A.*, *103*(34), 12,690–12,694, doi:10.1073/pnas.0602251103.

Qi, R., T. C. LaForce, and M. J. Blunt (2009), A three-phase four-component streamline-based simulator to study carbon dioxide storage, *Comput. Geosci.*, *13*(4), 493–509, doi:10.1007/s10596-009-9139-9.

Qin, J. F., R. J. Rosenbauer, and Z. Duan (2008), Experimental measurements of vapor-liquid equilibria of the H_2O+CO_2+CH_4 ternary system, *J. Chem. Eng. Data*, *53*(6), 1246–1249, doi:10.1021/je700473e.

Ruppel, C., and J. W. Pohlman (2008), Climate change and the global carbon cycle: Perspectives and opportunities, *NETL Methane Hydrate Newsl. Fire Ice*, *8*(3), 5. (Available at http://www.netl.doe.gov/technologies/oil-gas/publications/Hydrates/Newsletter/HMNewsWinter08.pdf#page = 5)

Santamarina, J. C., and J. Jang (2009), Gas production from hydrate bearing sediments: Geomechanical implications, *NETL Methane Hydrate Newsl. Fire in the Ice*, *9*(4). (Available at http://www.netl.doe.gov/technologies/oil-Gas/FutureSupply/MethaneHydrates/newsletter/newsletter.htm)

Seo, Y. T., and H. Lee (2001), Multiple-phase hydrate equilibria of the ternary carbon dioxide, methane, and water mixtures, *J. Phys. Chem. B*, *105*(41), 10,084–10,090, doi:10.1021/jp011095+.

Servio, P., and P. Englezos (2003), Morphology of methane and carbon dioxide hydrates formed from water droplets, *AIChE J.*, *49*(1), 269–276, doi:10.1002/aic.690490125.

Sloan, E. D., and C. A. Koh (2008), *Clathrate Hydrates of Natural Gases*, 3rd ed., 701 pp., CRC Press, Boca Raton, Fla.

Span, R., and W. Wagner (1996), A new equation of state for carbon dioxide covering the fluid region from the triple-point temperature to 1100 K at pressures up to 800 MPa, *J. Phys. Chem. Ref. Data*, *25*(6), 1509–1596.

Spycher, N., K. Pruess, and J. Ennis-King (2003), CO_2-H_2O mixtures in the geological sequestration of CO_2. I. Assessment and calculation of mutual solubilities from 12 to 100°C and up to 600 bar, *Geochim. Cosmochim. Acta*, *67*(16), 3015–3031, doi:10.1016/S0016-7037(03)00273-4.

Stern, L. A., S. H. Kirby, and W. B. Durham (1998), Polycrystalline methane hydrate: Synthesis from superheated ice, and low-temperature

mechanical properties, *Energy Fuels*, *12*(2), 201–211, doi:10.1021/ef970167m.

Stevens, C. J., J. J. Howard, B. A. Baldwin, G. Ersland, J. Husebø, and A. Graue (2008), Experimental hydrate formation and gas production scenarios based on CO2 sequestration, paper presented at Proceedings of the 6th International Conference on Gas Hydrates, Vancouver, B. C., Canada.

Subramanian, S., and E. D. Sloan (2002), Solubility effects on growth and dissolution of methane hydrate needles, paper presented at Fourth International Conference on Gas Hydrates, Yokohama, Japan.

Sun, R., and Z. H. Duan (2005), Prediction of CH_4 and CO_2 hydrate phase equilibrium and cage occupancy from ab initio intermolecular potentials, *Geochim. Cosmochim. Acta*, *69*(18), 4411–4424, doi:10.1016/j.gca.2005.05.012.

Sun, R., and Z. H. Duan (2007), An accurate model to predict the thermodynamic stability of methane hydrate and methane solubility in marine environments, *Chem. Geol.*, *244*(1–2), 248–262, doi:10.1016/j.chemgeo.2007.06.021.

Svandal, A., B. Kvamme, L. Gràànàsy, T. Pusztai, T. Buanes, and J. Hove (2006), The phase-field theory applied to CO_2 and CH_4 hydrate, *J. Cryst. Growth*, *287*(2), 486–490, doi:10.1016/j.jcrysgro.2005.11.071.

Tanaka, Y., N. Yamachi, S. Matsumoto, S. Kaneko, S. Okabe, and M. Shibuya (2008), Thermodynamic and transport properties of CO_2, CO_2-O_2, and CO_2-H_2 mixtures at temperatures of 300 to 30,000 K and pressures of 0.1 to 10 MPa, *Electr. Eng. Jpn.*, *163*(4), 18–29, doi:10.1002/eej.20467.

Thomas, W. J., and M. J. Adams (1965), Measurement of diffusion coefficients of carbon dioxide and nitrous oxide in water and aqueous solutions of glycerol, *Trans. Faraday Soc.*, *61*(508P), 668, doi:10.1039/tf9656100668.

Trusler, J. P. M., and M. Zarari (1992), The speed of sound and derived thermodynamic properties of methane at temperatures between 275 K and 375 K and pressures up to 10 MPa, *J. Chem. Thermodyn.*, *24*(9), 973–991, doi:10.1016/S0021-9614(05)80008-4.

Uchida, T., T. Ebinuma, J. Kawabata, and H. Narita (1999), Microscopic observations of formation processes of clathrate-hydrate films at an interface between water and carbon dioxide, *J. Cryst. Growth*, *204*(3), 348–356, doi:10.1016/S0022-0248(99)00178-5.

Vesovic, V., W. A. Wakeham, G. A. Olchowy, J. V. Sengers, J. T. R. Watson, and J. Millat (1990), The transport properties of carbon dioxide, *J. Phys. Chem. Ref. Data*, *19*(3), 763–808, doi:10.1063/1.555875.

Waite, W. F., L. A. Stern, S. H. Kirby, W. J. Winters, and D. H. Mason (2007), Simultaneous determination of thermal conductivity, thermal diffusivity and specific heat in sI methane hydrate, *Geophys. J. Int.*, *169*(2), 767–774, doi:10.1111/j.1365-246X.2007.03382.x.

Waite, W. F., et al. (2009), Physical properties of hydrate-bearing sediments, *Rev. Geophys.*, *47*, RG4003, doi:10.1029/2008RG000279.

Walsh, M. R., C. A. Koh, E. D. Sloan, A. K. Sum, and D. T. Wu (2009), Microsecond simulations of spontaneous methane hydrate nucleation and growth, *Science*, *326*(5956), 1095–1098, doi:10.1126/science.1174010.

Witherspoon, P. A., and L. Bonoli (1969), Correlation of diffusion coefficients for paraffin, aromatic, and cycloparaffin hydrocarbons in water, *Ind. Eng. Chem. Fundam.*, *8*(3), 589–591, doi:10.1021/i160031a038.

Yoon, J. H., Y. Yamamoto, T. Komai, H. Haneda, and T. Kawamura (2003), Rigorous approach to the prediction of the heat of dissociation of gas hydrates, *Ind. Eng. Chem. Res.*, *42*(5), 1111–1114, doi:10.1021/ie020598e.

Yoon, J. H., et al. (2004), Transformation of methane hydrate to carbon dioxide hydrate: In situ Raman spectroscopic observations, *J. Phys. Chem. A*, *108*(23), 5057–5059, doi:10.1021/jp0496831.

Zhou, X. T., et al. (2008a), Determination of appropriate condition on replacing methane from hydrate with carbon dioxide, *Energy Convers. Manage.*, *49*(8), 2124–2129, doi:10.1016/j.enconman.2008.02.006.

Zhou, X. T., et al. (2008b), Replacement of methane from quartz sand-bearing hydrate with carbon dioxide-in-water emulsion, *Energy Fuels*, *22*(3), 1759–1764, doi:10.1021/ef700705y.

D. N. Espinoza, J. W. Jung (corresponding author), and J. C. Santamarina, School of Civil and Environmental Engineering, Georgia Institute of Technology, 790 Atlantic Dr., NW, Atlanta, GA 30332-0355, USA. (jjung7@mail.gatech.edu)